

Oxido-Metal Complexes

Synthesis, Theoretical Study and Catalytic Application of Oxidometal (Mo or V) Complexes: Unexpected Coordination Due to Ligand Rearrangement through Metal-Mediated C–C Bond Formation

Sagarika Pasayat,^[a] Michael Böhme,^[b] Sarita Dhaka,^[c] Subhashree P. Dash,^[a,d] Sudarshana Majumder,^[a] Mannar R. Maurya,^[c] Winfried Plass,^{*[b]} Werner Kaminsky,^[e] and Rupam Dinda^{*[a]}

Dedicated to Professor Ekkehardt Fluck on the occasion of his 85th birthday

Abstract: Two novel dioxidomolybdenum(VI) complexes [MoO₂L¹] (**1**) and [MoO₂L²] (**2**) containing the MoO₂²⁺ motif with unexpected coordination motifs due to ligand rearrangement through Mo-mediated interligand C–C bond formation are reported. The ligands (H₂L^{1–2}) are tetradentate C–C-coupled O₂N₂-donor systems formed in situ during synthesis of the complexes by reaction of [Mo^{VI}O₂(acac)₂] with Schiff base ligands of 2-aminophenol with 2-pyridinecarbaldehyde (HL¹) and 2-quinolinecarbaldehyde (HL²). To confirm that the ligand rearrangement is assisted by molybdenum, the corresponding va-

nadium complexes [VO₂L¹] (**3**) and [VO₂L²] (**4**) containing original Schiff base ligand (HL^{1,2}) are also reported here. All complexes **1–4** are characterized by several physicochemical techniques and the structural features of **1** and **2** have been solved by X-ray crystallography. The proposed mechanism of molybdenum-mediated interligand C–C bond formation is supported by DFT calculations including the comparisons with the synthesized vanadium analogues. The catalytic potentials of **1–4** for the epoxidation of styrene and cyclohexene have also been explored.

Introduction

The coordination chemistry of transition metal complexes with nitrogen–oxygen donor ligands has become an interesting area of research in recent times. The ability of such complexes to possess unusual configurations, be structurally labile, and to be sensitive to molecular environments has inspired this high level of interest.^[1] Many transition metal complexes of Schiff base ligands have received considerable attention in biological fields; possible applications as antibacterial^[2–4] and anticancer^[5] agents, including those with DNA-cleaving activities,^[6,7] as well as catalysts for polymerizations,^[8] olefin oxidations^[6] and

Suzuki–Miyaura couplings have been particularly exciting.^[7] On the other hand, the coordination chemistry of molybdenum has been a subject of enthusiastic research due to the presence of molybdenum in metalloenzymes^[8–10] in addition to its biochemical and catalytic importance.^[11–27] Catalytic applications of molybdenum complexes in organic transformations, particularly in the oxidation^[28] and epoxidation of alkenes,^[29] oxidative bromination of organic substrates,^[30] and the oxidation of sulfides^[31] have been well established. Similarly, the coordination chemistry of vanadium has been attracting increasing interest due to the viability of many vanadium complexes as models for the biological functions of vanadium^[32–35] in processes such as haloperoxidation,^[36,37] phosphorylation,^[38] insulin mimicking^[39–43] and nitrogen fixation.^[44] The chemistry of vanadium has also received considerable attention due to its catalytic importance.^[45]

Transition metal complexes of 2-aminophenol-based Schiff base ligands have been widely reported.^[46–51] However, reports of Schiff base ligands with carbonyl compounds such as 2-pyridine- and 2-quinolinecarbaldehyde have been scarce.^[52–54] These ligands are monoanionic, tridentate, and coordinate at the Mo^{VI} center of the precursor MoO₂(acac)₂ forming μ -oxido-molybdenum compounds [MoO₂(L¹)₂(μ -O)].^[55] However, there are also reports where the sixth coordination site is filled by a monodentate conjugate base of the protic reaction solvent or a halide.^[56] Metal carbonyl complexes of Schiff bases derived

[a] Department of Chemistry, National Institute of Technology, Rourkela 769008 Odisha, India
E-mail: rupamdinda@nitrkl.ac.in
<https://sites.google.com/site/drrupamdinda/>

[b] Institute of Inorganic and Analytical Chemistry, Chair of Inorganic Chemistry II, Friedrich Schiller University Jena, Humboldtstr. 8, 07743 Jena, Germany
E-mail: sekr.plass@uni-jena.de
<http://www.plass.uni-jena.de/>

[c] Department of Chemistry, Indian Institute of Technology Roorkee, Roorkee 247667, India

[d] Department of Chemistry, Indira Gandhi Institute of Technology, Sarang, Parjang, Dhenkanal 759146, India

[e] Department of Chemistry, University of Washington, Box 351700, Seattle, WA 98195, USA

Supporting information and ORCID(s) from the author(s) for this article are available on the WWW under <http://dx.doi.org/10.1002/ejic.201501465>.

from 2-pyridinecarbaldehyde have been reported by Ali and co-workers, where the coordination site of the molybdenum complexes has been satisfied by terminal and bridging CO groups.^[57] Recently, Prasad and co-workers reported on oxido-vanadium(IV) complexes, $[\text{VO}(\text{L})(\text{B})](\text{ClO}_4)$ of *N*-2-pyridylmethylidene-2-hydroxyphenylamine (HL) Schiff base with phenanthroline bases as co-ligand.^[58] Oxidovanadium(V) complexes that mimic the active site of vanadium haloperoxidases with azomethine ligands have been reported by Pooransingh and co-workers.^[59]

Organic transformations of ligands involving the imine bond of transition metal complexes have generated renewed interest in recent years.^[60] Early reports by Golding and co-workers have shown that acetylacetonone can undergo a condensation with pyruvylidinatotetrammincobalt(III) ion.^[61] Additionally, Stark et al. have reported the diastereoselective addition of nucleophiles and electrophiles to isoquinoline as mediated by a chiral rhenium Lewis acid complex.^[62] Methylation of a tridentate ON_2 -donor Schiff base ligand of a palladium complex in the presence of nitromethane has been reported by Arnaiz et al.^[63] However, examples of such chemistry with oxidomolybdenum complexes are rare.^[64,65]

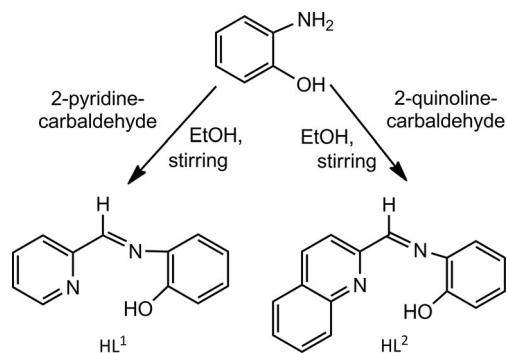
In the present report two novel dioxidomolybdenum(VI) complexes containing the MoO_2^{2+} motif are disclosed. In these cases, we have observed that the imine bond in the ligand undergoes rearrangement and a metal-mediated interligand C–C bond formation. The ligand transformations are initiated by a molybdenum-assisted C–C bond formation in the reaction medium. The chiral ligands (H_2L^{1-2}) are tetradentate C–C coupled O_2N_2 -donor systems formed in situ during synthesis of the complexes by reactions of bis(acetylacetonato)dioxidomolybdenum(VI) with Schiff base ligands resulting from condensation of 2-aminophenol with either 2-pyridinecarbaldehyde (to give ligand HL^1) or 2-quinolinecarbaldehyde (to give ligand HL^2). The reported dioxidomolybdenum(VI) complexes $[\text{MoO}_2\text{L}^{1'}]$ (**1**) and $[\text{MoO}_2\text{L}^{2'}]$ (**2**) coordinated with the O_2N_2 -donor rearranged ligand are expected to have improved Mo stability due to the +6 oxidation state relative to the corresponding ON_2 -donor ligand precursor.^[66] To confirm that the ligand rearrangement is assisted by molybdenum, corresponding vanadium complexes $[\text{VO}_2\text{L}^1]$ (**3**) and $[\text{VO}_2\text{L}^2]$ (**4**) with the Schiff base ligands (HL^1 and HL^2) are also reported here. Herein, we provide a more elaborate description of the underlying mechanism of transformation on the basis of DFT calculations. Moreover, the role of molybdenum in the ligand transformation is also elucidated with the aid of the synthesized vanadium analogues. All complexes **1–4** are fully characterized by several physicochemical techniques (IR, UV/Vis, NMR and ESI-MS) and the structural features of molybdenum complexes **1** and **2** have been solved by single-crystal X-ray crystallography. The catalytic potentials of **1–4** in the epoxidation of styrene and cyclohexene are also explored.

Results and Discussion

Synthesis

The precursor ligands ($\text{HL}^{1,2}$) were synthesized by condensation of equimolar amounts of 2-aminophenol and corresponding

carbonyl compounds [2-pyridine- (HL^1) and 2-quinolinecarbaldehyde (HL^2)] in absolute ethanol at room temperature (Scheme 1). Detailed methods used for the syntheses of precursor ligands ($\text{HL}^{1,2}$) and corresponding oxidometal complexes **1–4** are given in the experimentals section. Reactions of the 2-aminophenol-based ligands ($\text{HL}^{1,2}$) with $[\text{MoO}_2(\text{acac})_2]$ proceed in refluxing ethanol and afford yellow complexes $[\text{MoO}_2\text{L}^{1'}]$ (**1**) and $[\text{MoO}_2\text{L}^{2'}]$ (**2**) in moderate yields (Scheme 2). The rearranged ligands ($\text{H}_2\text{L}^{1,2}$) are formed (Scheme 3) as a result of templated reactions between one of the metal coordinated acetylacetonates in $[\text{MoO}_2(\text{acac})_2]$ and the corresponding Schiff base ligand ($\text{HL}^{1,2}$). These ligand transformations are highly specific and found to be initiated by a Mo-mediated C–C bond formation in the reaction medium. This is discussed in the latter section on computational studies. To confirm the reaction mechanism of this molybdenum-assisted organic rearrangement, the corresponding vanadium complexes were prepared following a similar approach, using the above mentioned ligands ($\text{HL}^{1,2}$), and $[\text{VO}(\text{acac})_2]$ as the metal precursor. It was observed that corresponding vanadium complexes $[\text{VO}_2\text{L}^1]$ (**3**) and $[\text{VO}_2\text{L}^2]$ (**4**) did not initiate the type of ligand rearrangement seen in the Mo scenarios (Scheme 2). All compounds were found to be highly soluble in aprotic solvents, (viz. DMF or DMSO) and only sparingly soluble in alcohol, CH_3CN and CHCl_3 . It was determined that the complexes are diamagnetic, indicating the presence of molybdenum in the +6 (for **1** and **2**) oxidation state whereas the vanadium is in the +5 (for **3** and **4**) oxidation state; both metal systems are non-conducting in solution. The detailed characterization of all complexes is presented in the respective section (IR, UV/Vis, NMR, ESI-MS and X-ray crystallography).

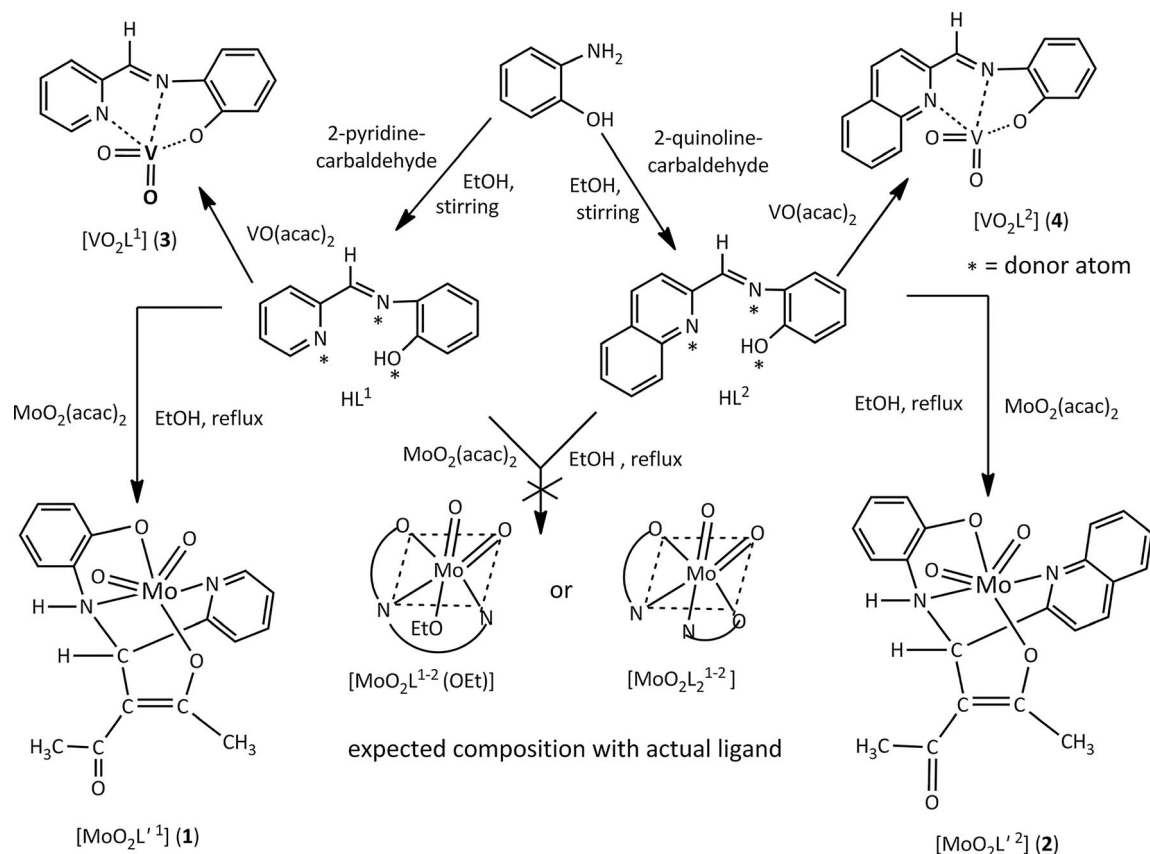


Scheme 1. Synthesis of tridentate Schiff base ligands ($\text{HL}^{1,2}$).

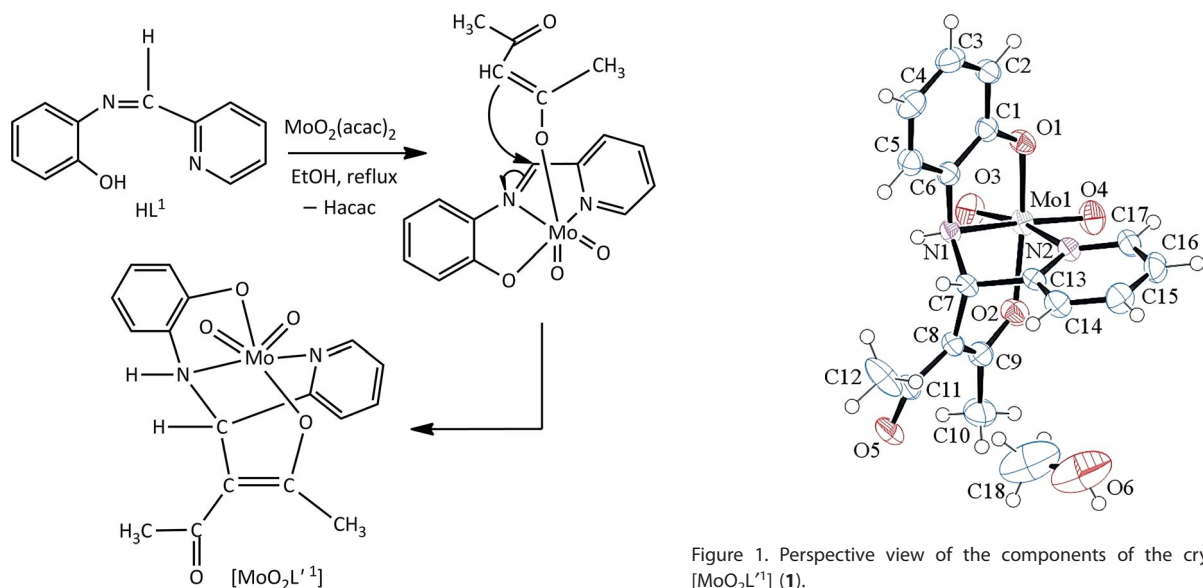
X-ray Structure Description

The structures of $[\text{MoO}_2\text{L}^{1'}]$ (**1**) (Figure 1) and $[\text{MoO}_2\text{L}^{2'}]$ (**2**) (Figure 2) reveal an unexpected coordination due to ligand rearrangement, which amounts to an interligand C–C bond coupling between two methylenic carbon atoms C7 and C8, leading to the formation of novel dioxidomolybdenum(VI) complexes.

In the both complex **1** and **2**, each corresponding rearranged ligand $\text{H}_2\text{L}^{1,2}$ is coordinated to molybdenum as a dianionic tetradentate N_2O_2 -donor, forming one six-membered and two



Scheme 2. Synthesis of dioxidomolybdenum(VI) complexes $[\text{MoO}_2\text{L}^1]$ (**1**) and $[\text{MoO}_2\text{L}^2]$ (**2**) and dioxidovanadium(V) complexes $[\text{VO}_2\text{L}^1]$ (**3**) and $[\text{VO}_2\text{L}^2]$ (**4**).



Scheme 3. Synthesis of C–C σ bonded rearranged ligands.

five-membered rings with bite angles of about 81° , 77° and 70° , respectively. The complexes (**1** and **2**) each have a six-coordinate distorted octahedral geometry where Mo–O(3) and Mo–O(4) bond lengths of the MoO_2^{2+} group are unexceptional^[11,51] and almost equal to a distance of about 1.70 Å. Complex **1** contains one methanol molecule per two molecules of metal

Figure 1. Perspective view of the components of the crystallography of $[\text{MoO}_2\text{L}^1]$ (**1**).

complex as the solvent of crystallization. The Mo–O and Mo–N distances are close to typical values.^[11,51] The relevant bond lengths and angles are summarized below in Table 1.

Both molecules are found to be involved in intermolecular hydrogen bonding. Two $[\text{MoO}_2\text{L}^1]$ (**1**) molecules form a dimeric unit via a pair of reciprocal H-bonds between the N1–H proton of one molecule and the acetylacetonate oxygen O5 of the other moiety. Similarly, N1–H of complex **2** reciprocally bonds

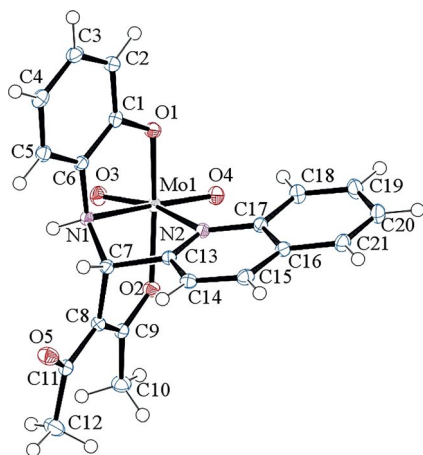


Figure 2. Perspective view of the components of the crystallography of $[\text{MoO}_2\text{L}^2]$ (**2**).

Table 1. Selected bond lengths [Å] and angles (°) for complex **1** and **2**.

	1	2
Bond lengths		
Mo1–O1	1.9452(15)	1.941(10)
Mo1–O2	1.9807(16)	1.953(10)
Mo1–O3	1.7023(16)	1.711(11)
Mo1–O4	1.6966(16)	1.703(10)
Mo1–N1	2.3252(18)	2.327(12)
Mo1–N2	2.3368(17)	2.417(12)
C7–C13	1.520(3)	1.507(18)
Bond angles		
O1–Mo1–O2	153.05(7)	152.89(4)
O1–Mo1–O3	99.96(8)	99.29(5)
O1–Mo1–O4	97.67(8)	97.71(5)
O1–Mo1–N1	76.34(6)	77.27(4)
O1–Mo1–N2	81.85(6)	81.20(4)
O2–Mo1–O3	95.93(8)	95.85(5)
O2–Mo1–O4	98.36(8)	99.33(5)
O2–Mo1–N1	80.95(6)	80.80(4)
O2–Mo1–N2	76.68(6)	76.44(4)
O3–Mo1–O4	106.87(8)	106.58(5)
O3–Mo1–N1	94.14(7)	88.50(5)
O3–Mo1–N2	162.67(7)	158.02(5)
O4–Mo1–N1	158.90(7)	164.77(4)
O4–Mo1–N2	89.85(7)	95.06(4)
N1–Mo1–N2	69.39(6)	70.08(4)

to O3 of the symmetry related molecule. On the other hand, further dimeric units of **2** are formed through a pair of van der Waals bonds formed between the oxido oxygen O4 of one molecule and the C3–H proton of the neighboring molecule as well as with O2 of the first molecule and the C4–H of the neighboring molecule; a second reciprocal intermolecular oxygen–hydrogen interaction exists between O5 and C7–H. The representative H-bonded dimeric structure of $[\text{MoO}_2\text{L}^1]$ (**1**) is given in Figure S1.

Spectral Characteristics

Spectral characteristics of both the ligands ($\text{HL}^{1,2}$) and complexes **1–4** are explained in the Exp. Section. The ligands exhibit

the IR band of minimum intensity in the 3164–3197 cm^{-1} region due to $\nu(\text{OH})$ stretching.^[43–49] Characteristic strong bands at around 1620 and 1580 cm^{-1} due to $\nu(\text{C}=\text{N})$ and $\nu(\text{C}=\text{C}/\text{aromatic})$ stretching modes, respectively,^[11,51] are observed in the spectra of both ligands and complexes. The appearance of new bands in the range 3080–3091 cm^{-1} in complexes **1** and **2** indicates the presence of –NH stretching which is absent in the case of ligand and vanadium complexes (**3** and **4**). A distinct peak at 3445 cm^{-1} in the IR spectra of complex **1** (Figure S2) indicates the presence of $\nu(\text{O}=\text{H})$ stretching due to the presence of CH_3OH (present as solvent of crystallization confirmed by X-ray crystallography) which is absent in the spectra of complex **2** (Figure S3). In addition, complexes (**1** and **2**) display a pair of sharp strong peaks in the range 907–931 cm^{-1} due to terminal $\nu(\text{Mo}=\text{O})$ stretching.^[11,36] In the case of dioxidovanadium complexes **3** and **4**, the presence of two strong bands in the range 930–956 cm^{-1} is assigned to V=O stretching, clearly indicating the dioxido nature of the complexes.

The electronic absorption spectra of complexes **1–4** were recorded in DMSO and found to be quite similar for all four complexes. The spectra display a shoulder in the 359–440 nm region and two strong absorptions in the 252–373 nm range are assignable to LMCT and intraligand transitions, respectively.^[11,51]

The ^1H NMR spectra of the free ligands exhibit a resonance in the range $\delta = 9.25$ – 9.36 ppm due to the phenolic OH and at $\delta = 8.71$ – 8.91 ppm due to the imine –CH protons respectively. All the aromatic protons from ligands are clearly observed in the expected region $\delta = 6.86$ – 8.69 ppm. The spectra of complexes **1** and **2** display two singlets in the range $\delta = 2.57$ – 2.59 ppm and $\delta = 2.22$ – 2.23 ppm which are attributable to the protons of the two methyl groups at C12 and C10 respectively present in the acetylacetonate fragment of the rearranged ligand.^[67] The N1–H and C7–H proton resonances are observed in the range $\delta = 8.68$ – 8.79 and $\delta = 5.81$ – 6.03 ppm, respectively.^[67] In the NMR spectra of complexes, the aromatic OH proton was not observed due to phenolic deprotonation.^[11,51]

The ^1H NMR of dioxidovanadium complexes **3** and **4** exhibit resonances in the range $\delta = 8.89$ – 9.26 ppm due to the imine proton. All aromatic protons of the complexes are clearly observed in the expected region, $\delta = 6.54$ – 8.87 ppm. The absence of peaks corresponding to the methyl groups and –NH group which were found in the molybdenum complexes supports the absence of any ligand rearrangement chemistry (**3**, Figure S4; **4**, Figure S5). The ^{51}V NMR spectra of **3** and **4** display resonances at $\delta = -499.4$ ppm and -498.3 ppm, respectively. These chemical shifts are typical for complexes containing a dioxidovanadium(V) species. A representative spectrum of **3** is shown in Figure S6.

In the ^{13}C NMR spectra of complexes **1** and **2**, signals for the aromatic carbons are found in the downfield region around $\delta_{\text{C}} = 116.01$ – 195.90 ppm while the resonances representative of the methyl groups of C10 and C12 within the acetylacetonate fragment of the rearranged ligands are found in the upfield region at around 23.90 ppm and 31.07 ppm, respectively. The signal for C(7), which is bonded to N1 and C8 via single bonds, also appears in the upfield region at $\delta_{\text{C}} = 63.71$ ppm. For com-

plexes **3** and **4**, the signals for the aromatic carbons appear in the range of $\delta_C = 111.93\text{--}210.39$ ppm.

ESI mass spectra of the complexes **1** and **2** have been recorded in methanol whereas for **3** and **4** mass spectra have been obtained in CH_3CN . Mass spectral analyses for **1** and **2** show the characteristic molecular ion peaks (M^+) at m/z 425.59 $[\text{M} - 0.5(\text{CH}_3\text{OH}) + \text{H}]^+$ and 475.17 $[\text{M} + \text{H}]^+$ respectively. For compounds **3** and **4**, ESI-MS peaks are observed at m/z 279.31 $[(\text{M} - \text{H})^+]$ and 333.07 $[\text{M} + 3\text{H}]^+$ respectively. Figures S7 and S8 show representative ESI mass spectra of **3** and **4**, respectively.

Electrochemical Properties

Electrochemical properties of complexes **1** and **2** as well as **3** and **4** have been studied by cyclic voltammetry in DMF and CH_3CN solution, respectively (0.1 M TBAP). Cyclic voltammetric data are summarized in Table 2 and the cyclic voltammograms of complexes **1–4** are displayed in Figure 3.

Table 2. Cyclic voltammetric results for dioxidomolybdenum(VI) (**1** and **2**) and dioxidovanadium(V) (**3** and **4**) complexes at 298 K.^[a]

	$E_{pc}/E_{1/2}$ (V)	ΔE_p (mV)
$[\text{MoO}_2\text{L}^1]$ (1)	-0.90, -1.31	-
$[\text{MoO}_2\text{L}^2]$ (2)	-0.94	420
$[\text{VO}_2\text{L}^1]$ (3)	-0.48	410
$[\text{VO}_2\text{L}^2]$ (4)	-0.86	320

[a] Solvents: DMF for **1** and **2**; CH_3CN for **3** and **4**; working electrode: glassy carbon; auxiliary electrode: platinum; reference electrode: saturated calomel electrode; supporting electrolyte: 0.1 M TBAP; scan rate: 50 mV/s. $E_{1/2} = (E_{pa} + E_{pc})/2$, where E_{pa} and E_{pc} are anodic and cathodic peak potentials vs. SCE, respectively. $\Delta E_p = E_{pa} - E_{pc}$.

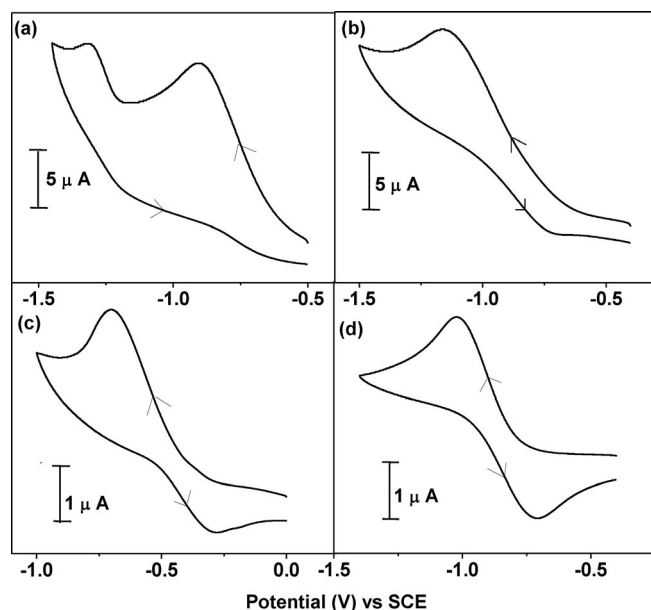


Figure 3. Cyclic voltammograms of **1–4**: (a) $[\text{MoO}_2\text{L}^1]$ (**1**), (b) $[\text{MoO}_2\text{L}^2]$ (**2**), (c) $[\text{VO}_2\text{L}^1]$ (**3**), and (d) $[\text{VO}_2\text{L}^2]$ (**4**).

The CV trace of complex **1** exhibits two single electron irreversible reductive responses at -0.90 V and -1.31 V [Figure 3 (a)] with respect to saturated calomel electrode, of which the first can be assigned to a metal-centered reduction of

$\text{Mo}^{\text{VI}} \rightarrow \text{Mo}^{\text{V}}$,^[11a,11b] whereas the second peak might be due to a ligand-centered reduction. For the CV trace of complex **2** only one single electron quasi-reversible reductive response at $E_{1/2}$ value of -0.94 V is observed [Figure 3 (b)], corresponding to the reduction of $\text{Mo}^{\text{VI}} \rightarrow \text{Mo}^{\text{V}}$.^[11a,11b] Vanadium complexes **3** and **4** exhibit a single electron quasi-reversible reductive response at $E_{1/2}$ values within the potential window -0.86 to -0.48 V [Figure 3 (c) and (d)] which can be attributed to the reduction of $\text{V}^{\text{V}} \rightarrow \text{V}^{\text{IV}}$.^[11c,11d] Single electron processes were verified by comparing the current height of the quasi-reversible reductive response with that of the standard ferrocene–ferrocenium couple under identical experimental conditions.

Computational Studies

The computational studies are based on density functional theory (DFT) and are focused on two aspects, firstly, to find a plausible reaction pathway for the C–C coupling that appears in **1** and **2**, and secondly, to explain possible differences in chemical behavior between the molybdenum(VI) and vanadium(V) complexes. As a basis to address these points we have performed full geometry optimizations for **1** and **2** denoted as **T1–XRD** and **T2–XRD**, respectively. The smallest error in bond lengths was obtained using the TPSSh *meta*-hybrid functional. This is in accordance with the literature^[68] which highlights promising applications of TPSSh for bioinorganic compounds. A comparison of several employed density functionals and the resulting root mean square errors in bond lengths are summarized in Table S1.

As a starting point for the reaction pathway, hexacoordinate intermediate compound $[\text{MoO}_2\text{L}^1(\text{acac}-\kappa\text{O})]$ (denoted as **T1–IM1**; see Figure 4 for atom numbering scheme) is hypothesized and envisioned to result from ligand exchange of one equivalent of acetylacetonate (denoted as acac) by L^1 . On one hand, the additional acac ligand is necessary to compensate for the positive charge of the $[\text{MoO}_2\text{L}^1]^+$ complex fragment. On the other hand, the exchange of one η^2 -acac ligand by η^3 - L^1 would increase the coordination number to seven, which should be disfavored due to the strong influences of the two oxido groups. Therefore, the remaining acac ligand is assumed to be

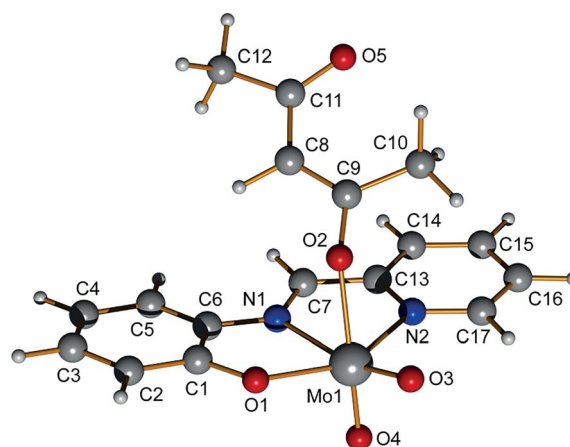
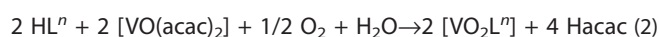


Figure 4. Structure and numbering scheme for intermediate species **T1–IM1**.

monodentate forming octahedral species **T1-IM1**. As an alternative for the intermediate species, we also considered the structure $[\text{MoO}_2(\text{HL}^1)(\text{acac-}\kappa\text{O})_2]$ (denoted as **T1-IML**; for structure see Figure S9), which might be generated by addition of the neutral ligand to the $[\text{MoO}_2(\text{acac})_2]$ starting complex. In **T1-IML** the two acac ligands are coordinated in a monodentate fashion leading to a hexacoordinate species. However, the calculated energy for **T1-IML** was found to be 11.54 kJ/mol higher than for **T1-IM1**. Consequently, we used **T1-IM1** as the starting point for the theoretical calculations, even though **T1-IML** has been discussed previously in the literature.^[65]

A corresponding hexacoordinate $[\text{VO}_2\text{L}^1(\text{acac-}\kappa\text{O})]^-$ species (formally denoted as **T3-IM1**) could not be found due to bond cleavage between the vanadium center and the acac ligand; this might be a significant factor in the different chemical behavior between the vanadium(V) and molybdenum(VI) species. Furthermore, the reactions given in Equation (1a), Equation (1b) and Equation (2) are related to different chemical conditions since the vanadium(IV) species needs to be oxidized to vanadium(V). Consequently, two neutral Hacac molecules are formed per equivalent of complex. In attempts to perform a corresponding C–C coupling of $[\text{VO}_2\text{L}^n]$ with a neutral Hacac molecule no stable minimum structure with a newly generated C7–C8 bond could be obtained. Because no oxidation is needed for molybdenum(VI) species **1** and **2**, a deprotonated acac ligand can remain coordinated, thus constituting the starting point for the theoretical reaction pathway.



A possible reaction pathway to generate **1** is shown in Figure 5 and corresponding structural parameters of the molybdenum center can be found in Table S2. Complex **2** was not investigated any further since it shows a similar chemical behavior and only a minor difference in the ligand system relative to **1**. In general, this mechanism can be divided into six elementary steps (denoted as steps I–VI in Figure 5); all steps entail only moderate activation barriers. Since the sp^2 hybridized carbon atom C7 in **T1-IM1** is prochiral the product of the C–C coupling is racemic. The chirality has no effect on the calculated properties, and thus, only the reaction pathway for the S enantiomer was investigated. In the reaction mechanism depicted, optimized intermediate minimum structures are denoted as **T1-IMn** whereas transition states are denoted as **T1-TSn**. Minimum structures and transition states were verified by corresponding frequency calculations giving none or exactly one imaginary frequency, respectively. To keep the model simple and computationally feasible it was important to limit its size and thus, additional solvent molecules were not included.

In the visualized mechanism the first step refers to the coupling of C7 and C8 which are already close to each other in **T1-IM1** with a distance of 3.083 Å due to coordination of the acac ligand. Despite this proximity, the coordination also has an effect on the negative charge distribution of the acac ligand. These changes can be shown by natural bond orbital population analysis (NPA) in Table S3. Significant changes, relative to an uncoordinated acac species, are observed for O2, O5, C8, and C11 indicating a decrease in their electron density. Nevertheless, these changes are small and the electron-withdrawing effect of the molybdenum center is weak due to an elongated Mo1–O2 bond with a length of 2.086 Å in **T1-IM1** as a result of the oxido group O4 in the *trans* position. Moreover, a significant electron-withdrawing effect is also observed for C7 of the ligand backbone which increases its electrophilicity relative to the corresponding carbon atom in a free deprotonated ligand species L¹ or L² (denoted in Table S3 as **L1** and **L2**, respectively). However, this increase is also obtained for the corresponding $[\text{VO}_2\text{L}^1]$ and $[\text{VO}_2\text{L}^2]$ species (denoted as **T3-IMO** and **T4-IMO**, respectively) and with similar magnitudes. Therefore, we conclude that the electron-withdrawing effect of the metal center does not drive the different chemical behavior. The calculated energy barrier for the C–C bond coupling is moderate (34.2 kJ/mol) and is related to a C7–C8 distance of 2.051 Å in the transition state **T1-TS1**. The corresponding transition state vector shows an imaginary frequency of $348i\text{cm}^{-1}$. The optimized C7–C8 bond length in resulting intermediate **T1-IM2** is 1.579 Å, which is slightly elongated relative to that in final complex **T1-XRD**. Formation of the new C7–C8 bond correlates to cleavage of the Mo1–O2 bond. These two structural changes lead to a considerable gain in energy relative to the transition state with a relative energy of 0.4 kJ/mol for **T1-IM2**.

To further proceed in the reaction pathway to final structure **T1-XRD**, a single proton transfer from C8 to N1 is needed. Attempts to perform this as an intramolecular proton transfer failed as this requires progression through an energetically unfavorable four-membered cyclic transition state. Moreover, along with this proton transfer, a major rearrangement in the ligand backbone is inevitable, including changes in hybridization at C8 and N1. Especially notable is the change at N1 to sp^3 hybridization; this is geometrically incompatible with an intramolecular proton transfer. However, it is well known that proton transfer processes are easily mediated by hydrogen-bonding networks through a von Grothuss-type mechanism.^[69,70] In particular, solvent-mediated proton transfer processes in methanol are related to small energy barriers as shown by ¹H NMR studies^[71] and theoretical calculations.^[72,73]

To mimic the required proton transfer we introduced a pyridine molecule as a sort of proton buffer capable of removing a proton from C8 in **T1-IM2** (Figure 5, step II and III) and also protonating N1 thus establishing final structure **T1-XRD** (Figure 5, step V and VI). Pyridine was chosen, since in the initial stage of the reaction the still present free ligand contains a 2-pyridyl moiety, which could easily act as an auxiliary base. The introduction of a pyridine molecule is associated with a decrease in the relative energy by –27.8 kJ/mol for the transition from **T1-IM2** to **T1-IM3**. As can be seen in Table S2, no signifi-

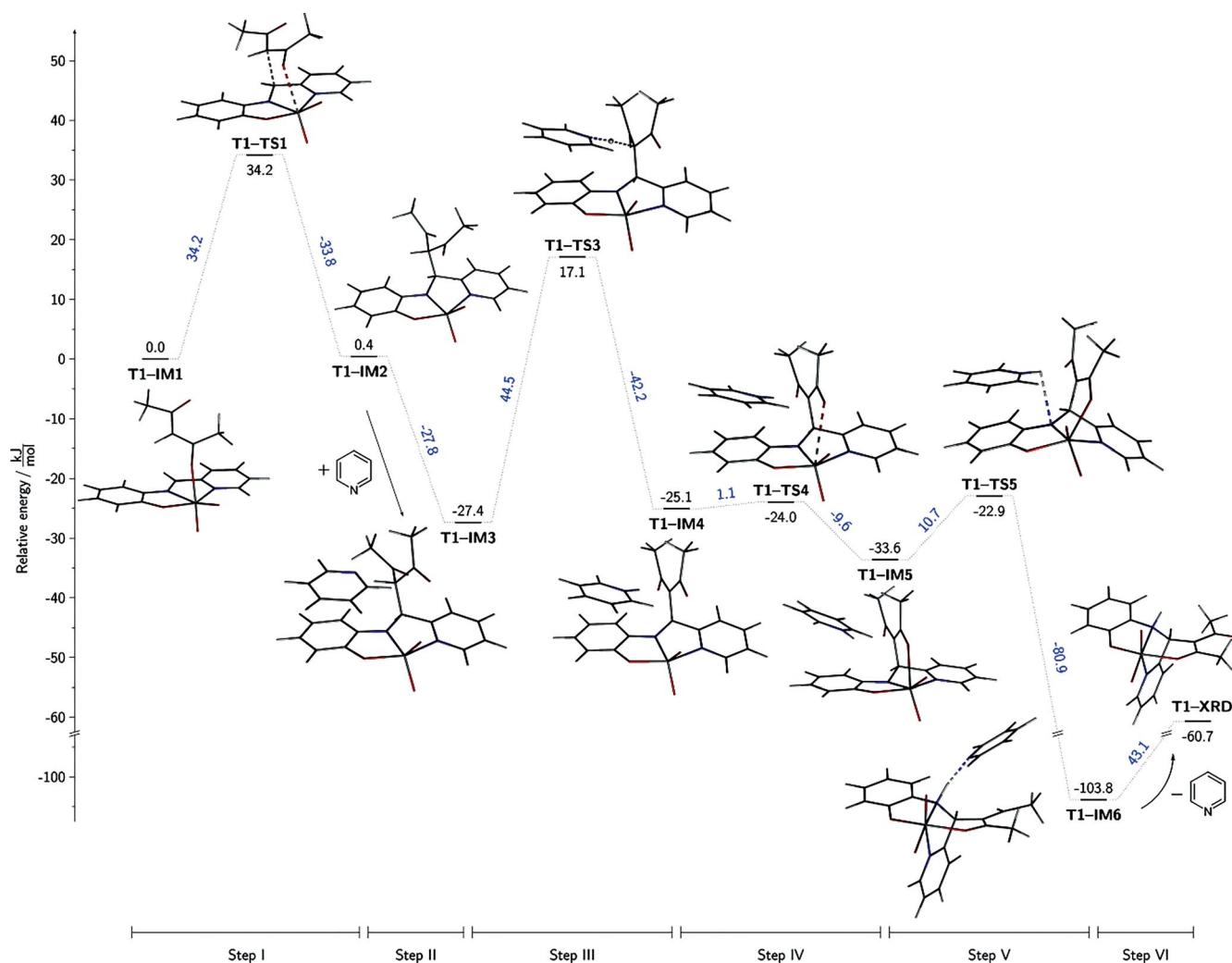


Figure 5. Hypothesized reaction mechanism leading to formation of $[\text{MoO}_2\text{L}^1]$ (**1**) (for notation and explanation see the text).

cant changes in bond lengths occur for the five donor atoms coordinated at the molybdenum center although an increase of the interatomic distance is observed for the atoms Mo1 and O2 (**T1-IM3**: 3.743 Å). Therefore, the energy gain in this step can be assigned to π - π interactions of the pyridine with the coordinated ligand (plane distance and angle: 3.5 Å and 4°) and weak hydrogen bonding between pyridine N atom and the hydrogen atom of the C8-H group ($\text{N}\cdots\text{H}$ 2.34 Å).

In step III the proton is transferred from C8 to the pyridine molecule with a relative transition state energy of 44.5 kJ/mol (**T1-TS3**). The relatively high barrier can be attributed to limitations of the computational model; this model excludes directed interactions with individual solvent molecules that might stabilize the transition state. However, no attempts have been made to decrease the activation barrier by extending the computational model. Consequently, this value represents an upper limit. Transition state **T1-TS3** exhibits a C8-H8 bond length of 1.402 Å and a high corresponding imaginary frequency of $1610i\text{cm}^{-1}$. The subsequent intermediate structure **T1-IM4**, with a protonated pyridine species, is lower in energy by -42.2 kJ/mol. Upon deprotonation, the C7-C8 bond length is

now slightly decreased (**T1-IM4**: 1.525 Å) which correlates well with a decrease in Mo1-N1 bond length (**T1-IM4**: 2.046 Å).

As a consequence of deprotonation in step III the negative charge at donor atom O2 increases (see Table S4) leading to elongation of the C2-O9 bond from 1.215 Å in **T1-IM3** to 1.260 Å in **T1-IM4** (see Table S5). Consequently, the stronger donor ability of O2 in **T1-IM4** initiates formation of the Mo1-O2 bond in step IV. Starting from **T1-IM4**, the large Mo1-O2 distance of 3.448 Å suggests an early transition state (**T1-TS4**: Mo1-O2 3.065 Å) associated with a low energy barrier (1.1 kJ/mol); this is in accordance with the calculated small imaginary frequency of $37i\text{cm}^{-1}$. Due to the structural *trans* effect of the oxido group O4, the newly formed coordinative bond Mo1-O2 is rather weak. This bond weakness is supported by a considerably elongated bond length (**T1-IM5**: 2.311 Å) relative to the corresponding Mo1-O1 bond in **T1-IM5** (1.959 Å) and may account for the relatively small energy gain in this reaction step.

The final structural rearrangement within the molybdenum coordination sphere *en route* to **T1-XRD** is related to the re-transfer of a proton from the pyridinium ion to anionic interme-

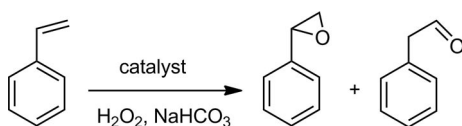
diate **T1-IM5**; this constitutes step V in Figure 5. The major structural changes are characterized by altering *cis/trans* positions of the donor atoms at the molybdenum center. This directly correlates with the change of N1 hybridization from a planar sp^2 to a tetrahedral sp^3 geometry leading to its increased basicity. Consequently, in transition state **T1-TS5**, a weak hydrogen bond to the pyridine molecule is observed (2.671 Å). In a concerted fashion with the structural changes, this proton is transferred to donor atom N1 during the transition from **T1-TS5** to **T1-IM6** and could not be separated as a single step. The structural rearrangement of the donor atoms can be described by increasing the O1-Mo1-O2 bond angle from 94.79° in **T1-IM5** to 151.70° in **T1-IM6** which corresponds to *cis* and *trans* configurations of the two donor atoms, respectively. For transition state **T1-TS5** a bond angle of 133.34° with a relative barrier of 10.7 kJ/mol and a corresponding imaginary frequency of $33i\text{cm}^{-1}$ are observed. The overall rearrangement *en route* to final structure **T1-XRD** results in *trans* positioning for the two oxido groups O3 and O4 relative to the weaker donor atoms N2 and N1, respectively. The rearrangement related to step V results in the largest energy gain (-80.9 kJ/mol) within the entire reaction mechanism. This takes into account the formation of a strong hydrogen bond with the pyridine ($\text{N}\cdots\text{H}$ 1.804 Å), which leads to the large overall driving force for the observed reaction.

In the last step the auxiliary pyridine molecule is removed, thus forming final species **T1-XRD**, which formally increases the energy by 43.1 kJ/mol; pyridine removal is the result of H-bond loss between the secondary amine proton and pyridine. Significant structural changes in bond lengths at the molybdenum center were not observed. However, this step is necessary to compare the energy gain of -60.7 kJ/mol in **T1-XRD** with respect to starting structure **T1-IM1**. Furthermore, in a polar solvent this energy gain might be even higher, since a new hydrogen-bond donor was generated at the expense of the non-polar C8-H8 bond.

Catalytic Epoxidation of Olefins

(a) Epoxidation of Styrene

Epoxidation of styrene catalyzed by oxidometal complexes **1-4** have been extensively studied using H_2O_2 as the oxidant.^[74,75] NaHCO_3 activates the hydrogen peroxide giving a peroxymono-carbonate moiety that assists in alkene epoxidation. Styrene, upon catalytic epoxidation, gave two products, namely styrene oxide (major) and phenyl acetaldehyde (minor) (Scheme 4). NaHCO_3 -assisted epoxidations of styrene have been reported in the literature and typically afford only styrene oxide as the product.^[76,77]



Scheme 4. Epoxidation of styrene with H_2O_2 .

We selected complex **1** as a representative catalyst and optimized epoxidation conditions for styrene by studying five dif-

ferent parameters. Specifically we evaluated: i) the effect of oxidant amounts (mols of H_2O_2 per mol of styrene), ii) amount of catalyst (per mol of styrene), iii) effect of inclusion of NaHCO_3 , iv) solvent effects, and v) impact of temperature. The effect of oxidant concentrations was studied by considering styrene: aqueous 30% H_2O_2 with molar ratios of 1:2, 1:3 and 1:4, where the mixture of styrene (0.520 g, 5 mmol), catalyst (1.1×10^{-3} mmol), NaHCO_3 (0.126 g, 1.5 mmol) and oxidant was dissolved in 5 mL of CH_3CN and the reaction was carried out at 60 °C.

As illustrated in Table S6 (Entries 2, 6, 7) and (Figure 6, panel a), the percent conversion of styrene improved from 46% to 94% upon increasing the styrene:oxidant ratio from 1:2 to 1:4 through 72% for 1:3, suggesting that 1:4 (styrene to H_2O_2) molar ratio is sufficient to achieve good conversions. Similarly, for three different amounts of **1** (0.56×10^{-3} , 1.1×10^{-3} and 1.7×10^{-3} mmol) at a styrene: H_2O_2 molar ratio of 1:4 under the reaction conditions noted above, it was found that 1.1×10^{-3} mmol catalyst gave 94% conversion while 0.56×10^{-3} mmol gave 62% and 1.7×10^{-3} mmol catalyst improved the conversion only slightly (96%) [Table S6 (Entries 1, 2, 3) and Figure 6, panel b]. The amount of NaHCO_3 also played a significant role in setting the conversion of styrene; the best conversion was obtained with 1.5 mmol of NaHCO_3 [Table S6 (Entries 2, 4, 5) and Figure 6, panel c]. Variations in the volume of CH_3CN (5, 7 and 10 mL) were also studied [Table S6 (Entries 2, 8, 9) and Figure 6, panel d], and it was observed that 5 mL of CH_3CN was sufficient to achieve good levels of epoxidation. Among the three different temperatures evaluated (40, 50 and 60 °C) for the fixed operating conditions of styrene (0.52 g, 5 mmol), H_2O_2 (2.27 g, 20 mmol), complex **1** (1.1×10^{-3} mmol), NaHCO_3 (0.126 g, 1.5 mmol) and CH_3CN (5 mL), running the reaction at 60 °C gave much better conversion [Table S6 (Entries 2, 10, 11) and Figure 6, panel e]. Thus, all reaction conditions, as concluded above [i.e. styrene (0.52 g, 5 mmol), H_2O_2 (2.27 g, 20 mmol), complex **1** (1.1×10^{-3} mmol), NaHCO_3 (0.126 g, 1.5 mmol), CH_3CN (5 mL) and $T = 60$ °C], were considered essential to achieving maximum transformation of styrene into a mixture of oxidation products. Table S6 and Figure 6 summarize all reaction conditions and resulting yields of styrene epoxidation.

The conversion of styrene and the selectivity of different reaction products using **1** as catalyst under the optimized reaction conditions (Table S6, Entry 2) have been analyzed as a function of time and are presented in Figure 7 and Table 3.

Thus, under the optimized reaction conditions, the selectivity of the two oxidation products varies in the order: styrene oxide (98.6%) > phenyl acetaldehyde (1.4%). Complexes **2**, **3** and **4** also follow the same order of product formation selectivity and with almost identical conversion values. Notably, a blank reaction devoid of any catalyst, under the same reaction conditions gave 32% conversion. This reaction, carried out at room temperature under the same conditions in the presence of NaHCO_3 , gave 11% conversion of styrene. Additionally, when this reaction was carried out under the same optimized conditions lacking NaHCO_3 , and containing either dioxidomolybdenum(VI) complexes **1** and **2**, or dioxidovanadium(V) complexes **3** and **4**

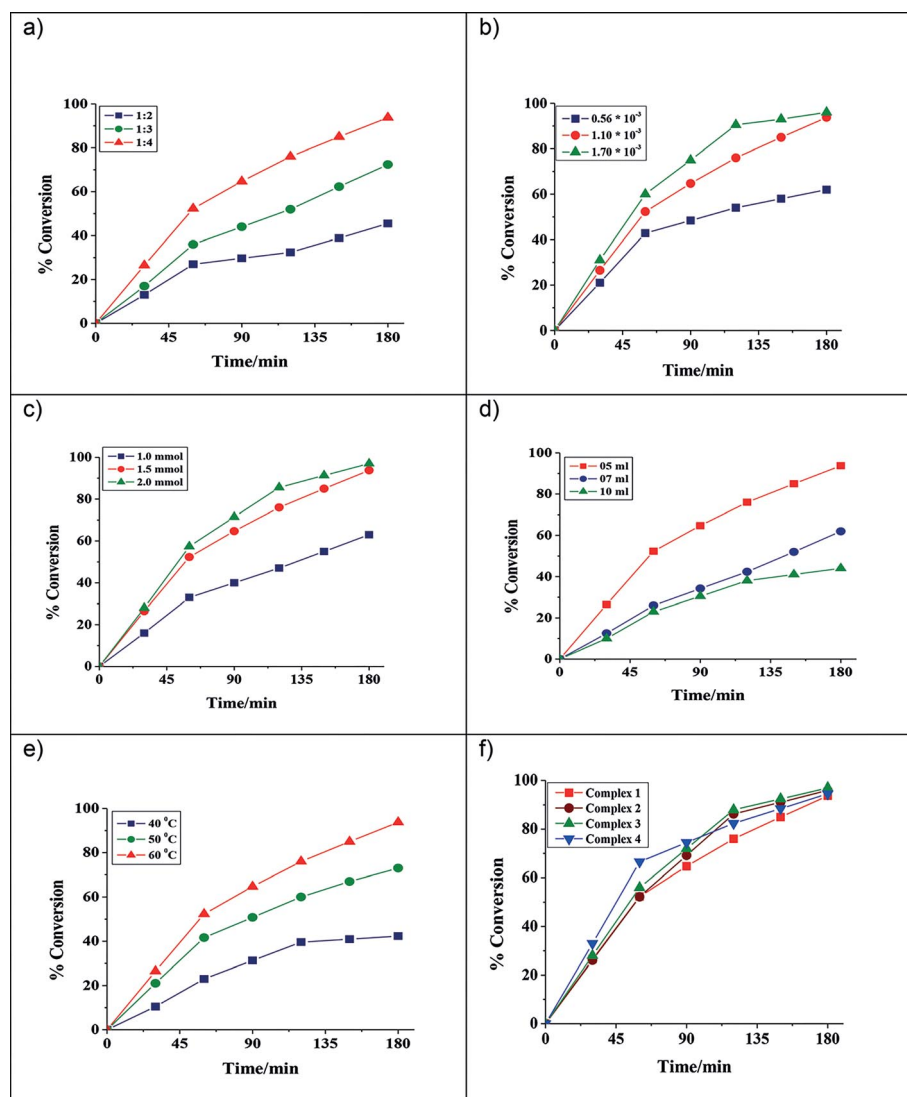


Figure 6. (a) Effect of oxidant amounts on the epoxidation of styrene. Reaction conditions: styrene (0.520 g, 5 mmol), catalyst $[\text{MoO}_2\text{L}^1]$ (**1**) (1.1×10^{-3} mmol), NaHCO_3 (0.126 g, 1.5 mmol), temperature 60°C and CH_3CN (5 mL). (b) Effect of catalyst amount on the epoxidation of styrene. Reaction conditions: styrene (0.520 g, 5 mmol), 30 % H_2O_2 (2.27 g, 20 mmol), NaHCO_3 (0.126 g, 1.5 mmol), temperature 60°C and CH_3CN (5 mL). (c) Effect of NaHCO_3 amount on the epoxidation of styrene. Reaction condition: styrene (0.520 g, 5 mmol), catalyst $[\text{MoO}_2\text{L}^1]$ (**1**) (1.1×10^{-3} mmol), 30 % H_2O_2 (2.27 g, 20 mmol), temperature 60°C and CH_3CN (5 mL). (d) Effect of solvent amount on the epoxidation of styrene. Reaction conditions: styrene (0.520 g, 5 mmol), 30 % H_2O_2 (2.27 g, 20 mmol), NaHCO_3 (0.126 g, 1.5 mmol), catalyst $[\text{MoO}_2\text{L}^1]$ (**1**) (1.1×10^{-3} mmol) and temperature 60°C (e) Effect of temperature on the epoxidation of styrene. Reaction conditions: styrene (0.520 g, 5 mmol), 30 % H_2O_2 (2.27 g, 20 mmol), NaHCO_3 (0.126 g, 1.5 mmol), catalyst $[\text{MoO}_2\text{L}^1]$ (**1**) (1.1×10^{-3} mmol) and CH_3CN (5 mL). (f) Plot showing conversion of all metal complexes.

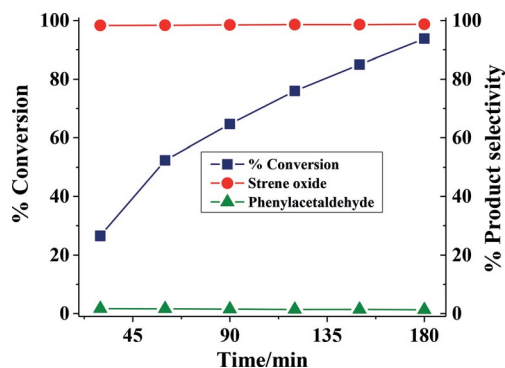


Figure 7. Plot showing conversion values and product selectivity as a function of time.

Table 3. Epoxidation of styrene, TOF and product selectivity using dioxidomolybdenum(VI) complexes $[\text{MoO}_2\text{L}^1]$ (**1**) and $[\text{MoO}_2\text{L}^2]$ (**2**) and dioxidovanadium(V) complexes $[\text{VO}_2\text{L}^1]$ (**3**) and $[\text{VO}_2\text{L}^2]$ (**4**) complexes as catalyst.

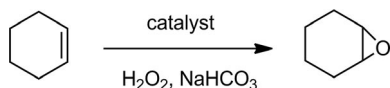
Catalyst	TOF [h^{-1}] ^[a]	Conv. [%]	Selectivity [%] ^[b]	
			phac	s.o.
1	1421	93.8	1.4	98.6
2	1600	96.0	1.5	98.5
3	951	97.0	1.4	98.6
4	1051	94.6	1.7	98.3
Blank reaction	–	32.0	4.0	96.0

[a] TOF values calculated at 3 h of reaction time. [b] s.o.: styrene oxide; phac: phenylacetaldehyde.

epoxidation conversions of 4–6 % or 19–23 % were obtained, respectively.

(b) Epoxidation of Cyclohexene

Complex **1** was also used as a representative catalyst to study epoxidation of cyclohexene by H_2O_2 . In this reaction NaHCO_3 was found to be necessary for catalytic activity to ensue. As shown in Scheme 5 these reactions gave only cyclohexene oxide.



Scheme 5. Epoxidation of cyclohexene with H_2O_2 .

In order to achieve optimum reaction conditions, three different cyclohexene to aqueous 30 % H_2O_2 molar ratios (1:2, 1:4 and 1:6) were considered for a fixed amount of cyclohexene

(0.41 g, 5 mmol), NaHCO_3 (0.126 g, 1.5 mmol) and catalyst (1.1×10^{-3} mmol) in 5 mL of CH_3CN . These reactions were carried out at 60 °C. As presented in Table S7 (Entries 1, 6, 7) and (Figure 8, panel a), a maximum of 46 % conversion was obtained at a cyclohexene to H_2O_2 molar ratio of 1:2 after 3 h. This conversion reached 94 % upon increasing this ratio to 1:4 while a 1:6 ratio improved the conversion slightly further (98 %). Under the operating conditions as described above [i.e. cyclohexene (0.41 g, 5 mmol), 30 % H_2O_2 (2.27 g, 20 mmol), NaHCO_3 (0.126 g, 1.5 mmol) in 5 mL of CH_3CN], the effect of catalyst identified by considering three different amounts (1.1×10^{-3} , 2.2×10^{-3} and 3.4×10^{-3} mmol) as a function of time was studied; results are illustrated in (Figure 8, panel b) (also see Table S7, Entries 1–3). It is clear from the plot that the use of 1.1×10^{-3} mmol catalyst provided excellent results allowing a maximum of 94 % conversion of cyclohexene. The use of

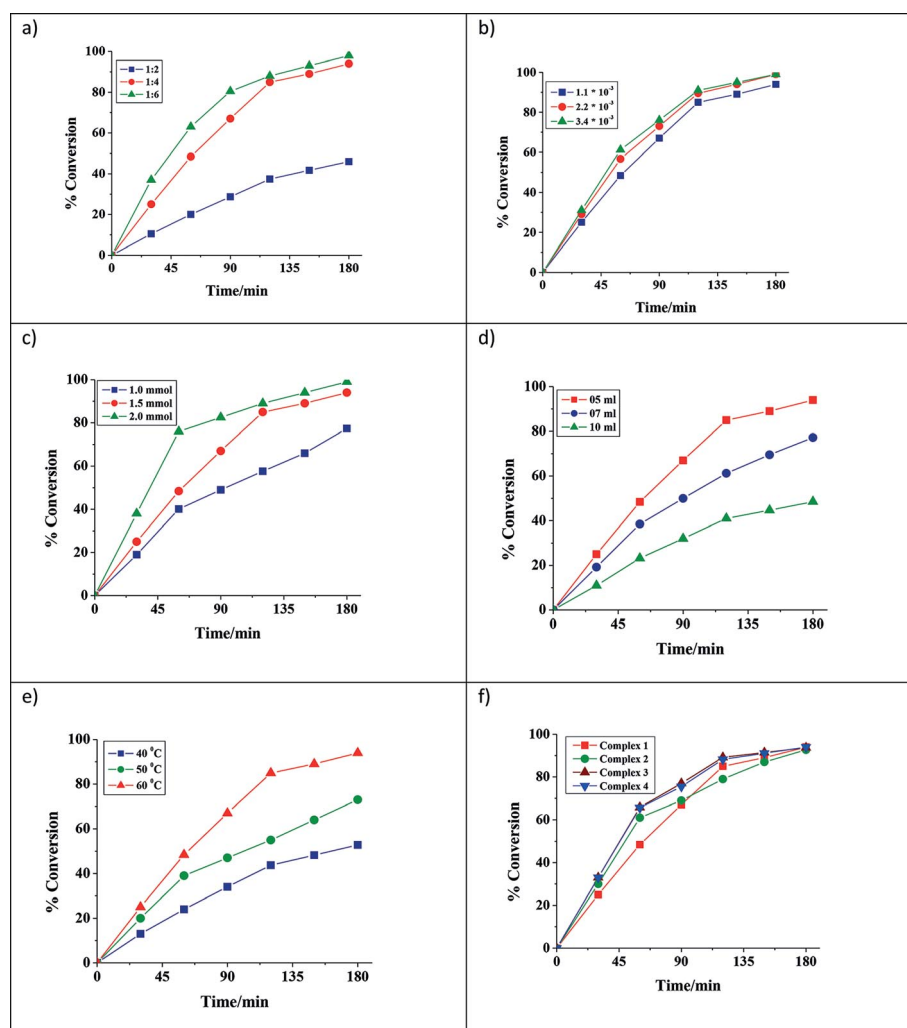


Figure 8. (a) Effect of oxidant amount on the epoxidation of cyclohexene. Reaction condition: cyclohexene (0.410 g, 5 mmol), catalyst $[\text{MoO}_2\text{L}^1]$ (**1**) (1.1×10^{-3} mmol), NaHCO_3 (0.126 g, 1.5 mmol), temperature 60 °C and CH_3CN (5 mL). (b) Effect of catalyst amount on the epoxidation of cyclohexene. Reaction conditions: cyclohexene (0.410 g, 5 mmol), 30 % H_2O_2 (2.27 g, 20 mmol), NaHCO_3 (0.126 g, 1.5 mmol), temperature 60 °C and CH_3CN (5 mL). (c) Effect of NaHCO_3 amount on the epoxidation of cyclohexene. Reaction condition: cyclohexene (0.410 g, 5 mmol), catalyst $[\text{MoO}_2\text{L}^1]$ (**1**) (1.1×10^{-3} mmol), 30 % H_2O_2 (2.27 g, 20 mmol), temperature 60 °C and CH_3CN (5 mL). (d) Effect of solvent amount on the epoxidation of cyclohexene. Reaction conditions: cyclohexene (0.410 g, 5 mmol), 30 % H_2O_2 (2.27 g, 20 mmol), NaHCO_3 (0.126 g, 1.5 mmol), catalyst $[\text{MoO}_2\text{L}^1]$ (**1**) (1.1×10^{-3} mmol) and temperature 60 °C (e) Effect of temperature on the epoxidation of cyclohexene. Reaction conditions: cyclohexene (0.410 g, 5 mmol), 30 % H_2O_2 (2.27 g, 20 mmol), NaHCO_3 (0.126 g, 1.5 mmol), catalyst $[\text{MoO}_2\text{L}^1]$ (**1**) (1.1×10^{-3} mmol) and CH_3CN (5 mL). (f) Plot showing conversion of all metal complexes.

2.2×10^{-3} and 3.4×10^{-3} mmol of catalysts showed only marginal improvements in conversion. We also optimized the amount of NaHCO_3 [Table S7, Entries 1, 4, 5 and Figure 8, panel c], the amount of CH_3CN solvent [Table S7, Entries 1, 8, 9 and Figure 8, panel d] and temperature [Table S7, Entries 1, 10, 11 and Figure 8, panel e] of the reaction and found that 1.5 mmol of NaHCO_3 , 5 mL of solvent and a reaction temperature of 60°C were sufficient to provide a 94 % conversion under the above reaction conditions. Table S7 and Figure 8 summarize all the conditions and conversions obtained under a particular set of conditions. In the absence of NaHCO_3 , 4–5 % and 21–24 % conversions of cyclohexene were obtained with dioxidomolybdenum(VI) **1** and **2** and dioxidovanadium(V) **3** and **4** complexes, respectively.

The conversion of cyclohexene and the selectivity of product formation using **1** as a catalyst under the optimized reaction conditions are presented in Table S7 (Entry 1), and under similar conditions for all complexes **1–4**, in Table 4. Thus, under the optimized reaction conditions (Table S7, Entry 1), other complexes **2–4** have also been tested for their ability to catalyze cyclohexene epoxidation. The reaction selectivity was found to be 100% in favor of cyclohexene oxide formation and the reaction was characterized by its high turnover frequency. A blank reaction (devoid of catalyst) using the above reaction conditions gave 36 % conversion. The epoxidation of cyclohexene under the same reaction conditions, but at carried out at room temperature, resulted in only 22 % conversion.

Table 4. Epoxidation of cyclohexene, TOF and selectivity cyclohexene oxide using different dioxidomolybdenum(VI) complexes [$\text{MoO}_2\text{L}'^1$] (**1**) and [$\text{MoO}_2\text{L}'^2$] (**2**) and dioxidovanadium(V) complexes [VO_2L^1] (**3**) and [VO_2L^2] (**4**) complexes as catalyst.

Catalyst	TOF [h^{-1}] ^[a]	Conv. [%]	Selectivity [%]
1	1424	94	100
2	1545	93	100
3	918	94	100
4	1044	94	100
Blank reaction	–	36	100

[a] TOF values calculated at reaction time of 3 h.

Reactivity of Complexes with H_2O_2 and Possible Reaction Intermediate

It is known that dioxidomolybdenum(VI) and dioxidovanadium(V) complexes react with H_2O_2 to give the corresponding oxido-peroxido complexes. The generation of such species has been established in DMSO by electronic absorption spectroscopy. In a typical reaction, 20 mL of ca. 10^{-4} M solution of complex **4** (as a representative catalyst) was treated with one drop of 30 % aqueous H_2O_2 (0.165 g, 1.5 mmol) dissolved in 5 mL of DMSO; the resultant spectroscopic changes are presented in Figure 9. There was found to be no change in band at 527 nm but the 370 nm band increased in intensity. A new band appeared at 305 nm while the bands at 260 nm and 271 nm significantly decreased in intensity. These changes indicate the interaction of complex **4** with H_2O_2 and formation of the anticipated oxido-peroxido species.

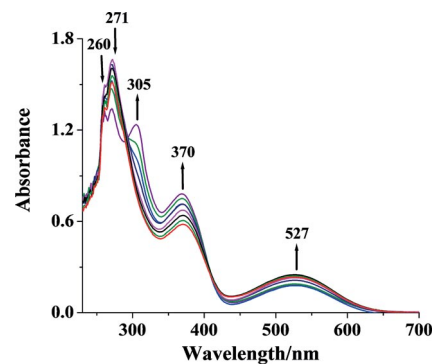
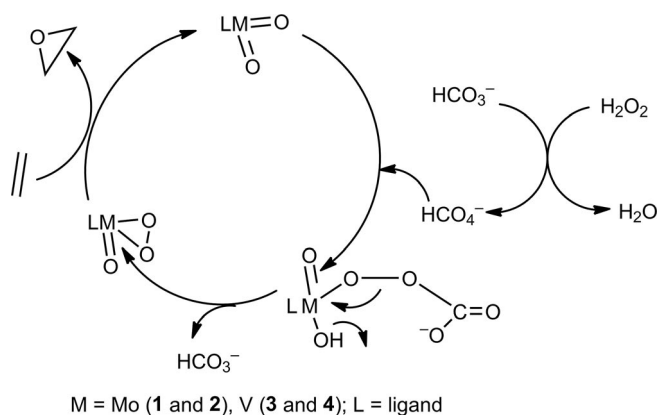


Figure 9. UV/Vis spectral changes observed during titration of [VO_2L^2] (**4**) with H_2O_2 .

To understand the possible reaction pathway during epoxidation chemistry, we also carried out a similar titration of **4** with H_2O_2 in the presence of NaHCO_3 . Upon addition of a few drops of a mixture of NaHCO_3 and H_2O_2 very similar spectral changes to those noted above were seen. Notably, the reaction of NaHCO_3 with H_2O_2 results in almost instant formation of HCO_4^- (peroxymonocarbonate)^[76] which accelerates generation of the oxido-peroxido intermediate relative to the reaction with H_2O_2 in the absence of NaHCO_3 . This intermediate enhances the transfer of oxygen to the substrate during catalytic epoxidation to give the final product. The exact mechanism for olefin epoxidation by oxidometal complexes in the presence of H_2O_2 is not clear at present. However, the formation of relevant oxido-peroxido complexes has been reported in the past.^[78] Although no attempts to isolate the appropriate intermediates for this system have been performed, based on the oxidation products obtained and experiments described above, a reaction pathway including oxido-peroxido intermediates can be rationally proposed (Scheme 6).



Scheme 6. Postulated reaction pathway for the epoxidation of olefins involving formation of an oxido-peroxido complex as is supported by reactions carried out herein.

Conclusions

Two novel dioxidomolybdenum(VI) complexes **1** and **2** containing C–C coupled rearranged ligands have been synthesized and successfully characterized. The C–C σ bond formation is highly specific and depends on the metal precursor [$\text{MoO}_2(\text{acac})_2$]. The

mechanism of the transformation has been established using DFT calculations. It has been validated that reactions using $[\text{VO}(\text{acac})_2]$ as a metal precursor do not initiate this type of ligand rearrangement. This was confirmed by the successful syntheses of corresponding dioxidovanadium complexes **3** and **4** and is in agreement with the theoretical results. The microanalysis, electrochemical study and spectroscopic characteristics are consistent with the molecular formula of all four reported complexes **1–4**. The molecular structures of dioxidomolybdenum(VI) complexes **1** and **2** have been confirmed by X-ray crystallography. Additionally, the catalytic potentials of **1–4**, in epoxidations of styrene and cyclohexene have also been explored; reactions of both substrates gave predominantly the corresponding oxides with high turnover frequencies. The intermediate peroxido species, expected to be involved during catalysis, has also been generated from a solution of **4** and studied by UV/Vis spectroscopy.

Experimental Section

Materials and Methods: $[\text{MoO}_2(\text{acac})_2]$ was prepared as described in the literature.^[79] Reagent grade solvents were dried and distilled prior to use. All other chemicals were reagent grade, available commercially and used as received. Commercially available TBAP (tetrabutylammonium perchlorate) was properly dried and used as a supporting electrolyte for recording cyclic voltammograms of the complexes. Elemental analyses were performed with a VarioELcube CHNS Elemental analyzer. IR spectra were recorded with a Perkin-Elmer Spectrum RXI spectrometer. NMR spectra were recorded with a Bruker UltraShield 400 MHz spectrometer at 298 K room temperature using SiMe_4 (^1H and ^{13}C) as an internal and VOCl_3 (^{51}V) as external standard. Electronic spectra were recorded using a Lambda25, Perkin-Elmer spectrophotometer. Magnetic susceptibility was measured with a Sherwood Scientific AUTOMSB sample magnetometer. Mass spectra were recorded with a SQ-300 MS instrument operating in ESI mode. A CH-Instruments (Model No. CHI6003E) electrochemical analyzer was used for cyclic voltammetric experiments with DMF (for **1** and **2**) and CH_3CN (for **3** and **4**) solutions of the complexes containing TBAP (tetra butyl ammonium perchlorate) as the supporting electrolyte. The three electrode measurements were carried out at 298 K with a glassy carbon working electrode, platinum auxiliary electrode and SCE as a reference electrode. **Caution:** Although no problems were encountered during the course of this work, attention is drawn to the potentially explosive nature of *perchlorates*.

A Shimadzu 2010 plus gas-chromatograph fitted with an Rtx-1 capillary column (30 m \times 0.25 mm \times 0.25 μm) and a FID detector was used to analyze the reaction products and their quantifications were made on the basis of the relative peak area of the respective product. The identity of the products was confirmed using a GC-MS model Perkin-Elmer, Clarus 500 and comparing the fragments of each product with the library available. The percent conversion of substrate and selectivity of products was calculated from GC data using the formulae:

$$\% \text{ Conversion of substrate} = 100 - \frac{\text{Peak area of a substrate}}{\text{Total area of substrate + products}} \times 100$$

$$\% \text{ Selectivity of a product} = \frac{\text{Peak area of a product}}{\text{Total area of products}} \times 100$$

Synthesis of Ligands (HL^{1,2}): Schiff base ligands HL¹ and HL² were prepared by the condensation of 2-aminophenol with 2-pyridine-

carbaldehyde (HL¹) and 2-quinolinecarbaldehyde (HL²) in equimolar ratios in ethanol following a standard procedure.^[80] The resulting brown compounds were filtered, washed with ethanol and dried with fused CaCl_2 .

HL¹: Yield 0.13 g (65 %). $\text{C}_{12}\text{H}_{10}\text{N}_2\text{O}$ (198.22): calcd. C 72.72, H 5.05, N 14.14; found C 72.76, H 5.07, N 14.09. FTIR (KBr): $\tilde{\nu} = 3197$ (O–H), 1622 (C=N), 1583 (C=C/aromatic) cm^{-1} . ^1H NMR (400 MHz, $[\text{D}_6]\text{DMSO}$): $\delta = 9.25$ (s, 1 H, OH), 8.71 (s, 1 H, CH), 6.86–6.69 (m, 8 H, aromatic) ppm. $^{13}\text{C}\{^1\text{H}\}$ NMR (100 MHz, $[\text{D}_6]\text{DMSO}$): $\delta = 159.33, 154.49, 151.37, 149.45, 136.82, 136.80, 128.21, 125.37, 121.49, 119.66, 119.57, 116.31$ ppm.

HL²: Yield 0.18 g (72 %). $\text{C}_{16}\text{H}_{12}\text{N}_2\text{O}$ (248.28): calcd. C 77.4, H 4.87, N 11.28; found C 77.38, H 4.89, N 11.26. FTIR (KBr): $\tilde{\nu} = 3164$ (O–H), 1611 (C=N), 1581 (C=C/aromatic) cm^{-1} . ^1H NMR (400 MHz, $[\text{D}_6]\text{DMSO}$): $\delta = 9.36$ (s, 1 H, OH), 8.91 (s, 1 H, CH), 6.87–8.58 (m, 10 H, aromatic) ppm. $^{13}\text{C}\{^1\text{H}\}$ NMR (100 MHz, $[\text{D}_6]\text{DMSO}$): $\delta = 167.79, 157.14, 154.32, 152.92, 136.86, 134.43, 132.44, 130.90, 129.52, 128.91, 127.88, 127.81, 120.38, 118.34, 116.29, 115.49$ ppm.

Synthesis of Complexes $[\text{MoO}_2\text{L}^{1,2}]$ (1** and **2**):** To the refluxing solution of 1.0 mmol ligand (HL^{1,2}) in 30 mL of ethanol, 1.0 mmol of $\text{MoO}_2(\text{acac})_2$ was added. The color of the solution changed to dark red. After 3 h, the resulting solution was filtered and slow evaporation of the filtrate over 2 d produced yellow colored crystals. The crystals were filtered and washed with ethanol and suitable single crystals were selected for X-ray analysis. A similar compound has recently been reported,^[65] although our work was already initiated earlier and had been reported in a Ph. D. thesis.^[81] However, we observed differences in the molecular structure associated with a solvent of crystallization, which is discussed in the X-ray crystallography section.

$[\text{MoO}_2\text{L}^1]$ (1**):** Yield 0.25 g (57 %). $\text{C}_{17}\text{H}_{16}\text{MoN}_2\text{O}_5 \cdot 0.5(\text{CH}_3\text{OH})$ (424.26): calcd. C 47.74, H 4.12, N 6.36; found C 47.72, H 4.13, N 6.35. FTIR (KBr): $\tilde{\nu} = 3080$ (N–H), 3445 (O–H), 1604 (C=N), 1256 (C–O)_{enolic}, 924, 907 (Mo=O) cm^{-1} . UV/Vis (DMSO): λ_{max} , nm (ϵ , $\text{dm}^3 \text{mol}^{-1} \text{cm}^{-1}$): 417 (30124), 320 (25123), 252 (16352). ^1H NMR (400 MHz, $[\text{D}_6]\text{DMSO}$): $\delta = 6.63$ –8.87 (m, 8 H, aromatic), 8.68 (s, 1 H, NH), 5.81 (s, 1 H, CH), 2.57 (s, 3 H, CH_3), 2.22 (s, 3 H, CH_3) ppm. $^{13}\text{C}\{^1\text{H}\}$ NMR (100 MHz, $[\text{D}_6]\text{DMSO}$): $\delta = 195.90, 173.66, 162.00, 157.43, 148.49, 141.49, 133.32, 129.55, 126.36, 125.50, 122.49, 121.16, 117.31, 116.29, 63.71, 31.39, 24.42$ ppm. ESI-MS: $m/z = 425.59$ $[\text{M} - 0.5(\text{CH}_3\text{OH}) + \text{H}]^+$.

$[\text{MoO}_2\text{L}^2]$ (2**):** Yield 0.31 g (65 %). $\text{C}_{21}\text{H}_{18}\text{MoN}_2\text{O}_5$ (474.32): calcd. C 53.16, H 3.83, N 5.90; found C 53.15, H 3.84, N 5.90. FTIR (KBr): $\tilde{\nu} = 3091$ (N–H), 1597 (C=N), 1253 (C–O)_{enolic}, 931, 910 (Mo=O) cm^{-1} . UV/Vis (DMSO): λ_{max} , nm (ϵ , $\text{dm}^3 \text{mol}^{-1} \text{cm}^{-1}$): 423 (30125), 329 (25126), 257 (16350). ^1H NMR (400 MHz, $[\text{D}_6]\text{DMSO}$): $\delta = 6.64$ –9.27 (m, 10 H, aromatic), 8.79 (s, 1 H, NH), 6.03 (s, 1 H, CH), 2.59 (s, 3 H, CH_3), 2.23 (s, 3 H, CH_3) ppm. $^{13}\text{C}\{^1\text{H}\}$ NMR (100 MHz, $[\text{D}_6]\text{DMSO}$): $\delta = 195.49, 174.28, 162.43, 158.44, 143.31, 141.18, 132.84, 131.48, 128.96, 128.44, 128.28, 127.43, 126.59, 125.63, 120.78, 119.58, 116.91, 116.01, 63.71, 30.75, 23.49$ ppm. ESI-MS: $m/z = 475.17$ $[\text{M} + \text{H}]^+$.

Complexes $[\text{VO}_2\text{L}^{1-2}]$ **3 and **4**:** To a stirring solution of 1.0 mmol of ligand HL^{1,2} in ethanol (30 mL) was added 1.0 mmol of $[\text{VO}(\text{acac})_2]$. The color of the solution changed to dark red. The mixture was then left to stir. After 1 h, red colored residue settled down in the reaction mixture, which was filtered and washed with ethanol.

$[\text{VO}_2\text{L}^1]$ (3**):** Yield 61 %. $\text{C}_{12}\text{H}_9\text{N}_2\text{O}_3\text{V}$ (280.16): calcd. C 51.40, H 3.81, N 10.00; found C 50.15, H 3.84, N 9.98. FTIR (KBr): $\tilde{\nu} = 1583$ (C=N), 947, 930 (V=O) cm^{-1} . UV/Vis (DMSO): λ_{max} , nm (ϵ , $\text{dm}^3 \text{mol}^{-1} \text{cm}^{-1}$):

359 (30125), 319 (14886), 275 (13024). ^1H NMR (400 MHz, $[\text{D}_6]\text{DMSO}$): δ = 9.26 (s, 1 H, CH), 6.69–8.87 (m, 8 H, aromatic) ppm. $^{13}\text{C}\{^1\text{H}\}$ NMR (100 MHz, $[\text{D}_6]\text{DMSO}$): δ = 210.39, 205.11, 185.34, 173.36, 165.41, 160.59, 155.42, 154.10, 147.77, 140.53, 132.17, 118.69 ppm. ^{51}V NMR ($[\text{D}_6]\text{DMSO}$): δ = –499.4 ppm. ESI-MS: m/z = 279.31 $[\text{M} - \text{H}]^+$, 301.28 $[\text{M} + \text{Na} - 2\text{H}]^+$.

[VO₂L²] (4): Yield 63%. C₁₆H₁₁N₂O₃V (330.22): calcd. C 58.18, H 3.33, N 8.48; found C 58.15, H 3.30, N 8.50. FTIR (KBr): $\tilde{\nu}$ = 1594 (C=N), 956, 947 (V=O) cm⁻¹. UV/Vis (DMSO): λ_{max} nm (ϵ , dm³ mol⁻¹ cm⁻¹): 440 (10433), 373 (25126), 293 (16250). ^1H NMR (400 MHz, $[\text{D}_6]\text{DMSO}$): δ = 6.54–8.54 (m, 10 H, aromatic), 8.89 (s, 1 H, CH) ppm. $^{13}\text{C}\{^1\text{H}\}$ NMR (100 MHz, $[\text{D}_6]\text{DMSO}$): δ = 203.85, 198.30, 152.16, 147.73, 147.35, 137.77, 137.33, 131.32, 130.99, 129.83, 129.04, 128.84, 127.84, 124.02, 120.64, 111.93 ppm. ^{51}V NMR ($[\text{D}_6]\text{DMSO}$): δ = –498.3 ppm. ESI-MS: m/z = 333.07 $[\text{M} + 3\text{H}]^+$.

Crystallography: Suitable single crystals of **1** and **2** were chosen for X-ray diffraction studies. Crystallographic data and details of refinement are given in Table 5. These compounds both crystallize in the triclinic space group $P\bar{1}$. The unit cell parameters and the intensity data were collected for complex **1** with a Bruker Smart Apex CCD diffractometer at about 293 K and for complex **2** at 100 K with a Bruker APEX II using graphite monochromated Mo- K_{α} radiation (λ = 0.71073 Å). The intensity data were corrected for Lorentz, polarization and absorption effects. The structures were solved using the SHELXS97^[82] and refined using the SHELXL97^[83] computer programs. The non-hydrogen atoms were refined anisotropically.

Table 5. Crystal and refinement data of complexes **1** and **2**.

	1	2
Formula	C ₃₅ H ₃₆ Mo ₂ N ₄ O ₁₁	C ₂₁ H ₁₈ MoN ₂ O ₅
M	880.56	474.31
Crystal symmetry	triclinic	triclinic
Space group	$P\bar{1}$	$P\bar{1}$
<i>a</i> [Å]	8.4739(5)	9.1187(19)
<i>b</i> [Å]	9.6684(5)	9.6426(19)
<i>c</i> [Å]	11.5506(7)	11.841(2)
α [°]	94.10(10)	73.432(8)
β [°]	109.95(10)	84.460(9)
γ [°]	96.81(10)	66.820(9)
<i>V</i> [Å ³]	876.87(9)	917.2(3)
<i>Z</i>	1	2
<i>D</i> _{calc} [g cm ⁻³]	1.668	1.717
μ (Mo- K_{α}) [mm ⁻¹]	0.782	0.753
<i>F</i> (000)	446	480
max./min.trans.	0.9546/0.9051	0.9285/0.8639
2 θ (max.) [°]	25.00	25.00
Reflections collected/unique	3434	4651
<i>R</i> ₁ ^[a] [<i>I</i> > 2 σ (<i>I</i>)]	0.0240	0.0188
<i>wR</i> ₂ ^[b] [all data]	0.0637	0.0498
<i>S</i> [goodness of fit]	1.078	1.067
min./max. resid. electron density (e Å ⁻³)	0.350/–0.288	0.435/–0.409

[a] $R_1 = \sum |F_o| - |F_c| / \sum |F_o|$. [b] $wR_2 = \{\sum [w(F_o^2 - F_c^2)^2] / \sum [w(F_o^2)^2]\}$.

CCDC 1436851 (for **1**) and 1436852 (for **2**) contain the supplementary crystallographic data for this paper. These data can be obtained free of charge from The Cambridge Crystallographic Data Centre.

Computational Details: The quantum chemical calculations were performed with the ORCA 3.0.3 package of programs.^[84] All calculations were employed with the *meta*-GGA hybrid functional by Tao, Perdew, Staroverov, and Scuseria,^[85] denoted as TPSSH. Triple- ζ def2-TZVPP basis sets were used for all atoms^[86] together with a

tight SCF energy convergence criterion (10^{-8} a.u.). Increasing the quality of the basis sets to quadruple- ζ did not result in any significant structural changes. Therefore, the triple- ζ def2-TZVPP basis sets give the balance between accuracy and computational time. Due to the lack of dispersion forces in DFT the atom-pairwise dispersion correction DFTD3 by Grimme^[87] was employed for all calculations. Furthermore, ethanol solvent effects were included with the conductor-like screening model (COSMO) by Klamt.^[88] Final energies for structures inclusive of pyridine within the computational model were corrected with the counterpoise method of Boys^[89] to minimize the basis set superposition error (BSSE). Natural Population Analyses have been performed with the Turbomole package of programs in version 6.6^[90] at the same level of theory.

Possible transition states for the reaction mechanism were located from a series of different linear transits which were based on optimized intermediate structures as starting geometries. For these linear transit calculations a constrained internal coordinate was defined whereas all other coordinates were optimized. The identified transition state guesses were checked by frequency calculations which gave exactly one imaginary frequency. This mode was verified to be the expected motion along the reaction coordinate. After performing the subsequent transition state optimizations the final transition states were again verified by frequency calculations.

Catalytic Epoxidation of Olefins

(a) Epoxidation of Styrene: In a typical reaction, styrene (0.52 g, 5 mmol) and aqueous 30% H₂O₂ (2.27 g, 20 mmol), NaHCO₃ (0.126 g, 1.5 mmol), were combined in CH₃CN (5 mL) and temperature of the reaction mixture was raised to 60 °C. The catalyst (1.1×10^{-3} mmol) was added to the above reaction mixture and stirred. Oxidized products were analyzed quantitatively by gas chromatograph during the reaction by withdrawing small aliquots of the reaction mixture at 30 min intervals. The identity of the products was confirmed by GC-MS. Various parameters, such as amounts of oxidant, catalyst, NaHCO₃ and solvent as well as temperature of the reaction medium were studied in order to understand their influence on conversion rates and selectivities achievable during the reaction.

(b) Epoxidation of Cyclohexene: Cyclohexene (0.41 g, 5 mmol), 30% H₂O₂ (2.27 g, 20 mmol), NaHCO₃ (0.126 g, 1.5 mmol) and catalyst (1.1×10^{-3} mmol) were mixed in CH₃CN (5 mL), and the reaction mixture was heated at 60 °C with continuous stirring. The reaction products were analyzed and identified as mentioned above for conversions involving styrene.

Supporting Information (see footnote on the first page of this article): Additional tables and figures of computational studies, ESI-MS and spectral information have been included as supporting information.

Acknowledgments

The authors thank the reviewers for their comments and suggestions, which were helpful in preparing the revised version of the manuscript. Funding of this research was provided by Council of Scientific and Industrial Research (CSIR), Government of India [grant number 01(2735)/13/EMR-II]. The authors acknowledge the use of a UV-Vis spectrophotometer purchased from Department of Science and Technology (DST), New Delhi (grant number SR/FT/CS-016/2008). S. P. gratefully acknowledges CSIR for a research fellowship.

Keywords: Molybdenum · Vanadium · Homogeneous catalysis · C–C coupling · Epoxidation · DFT studies · Ligand effects · Schiff bases

- [1] A. Golcu, M. Tumer, H. Demirelli, R. A. Wheatley, *Inorg. Chim. Acta* **2005**, 358, 1785–1797.
- [2] V. Patroniak, A. R. Stefankiewicz, J.-M. Lehn, M. Kubicki, *Eur. J. Inorg. Chem.* **2005**, 4168–4173.
- [3] A. Balamurugan, G. Balossier, D. Laurent-Maquin, S. Pina, A. H. S. Rebelo, J. Faure, J. M. F. Ferreira, *Dent. Mater.* **2008**, 24, 1343–1351.
- [4] Z. H. Chohan, S. Kausar, *Chem. Pharm. Bull.* **1993**, 41, 951–953.
- [5] M. Kurtoglu, F. Purtaş, S. Toroglu, *Transition Met. Chem.* **2008**, 33, 705–710.
- [6] P. K. Sasmal, A. K. Patra, A. R. Chakravarty, *J. Inorg. Biochem.* **2008**, 102, 1463–1472.
- [7] P. Prasad, P. K. Sasmal, R. Majumdar, R. R. Dighe, A. R. Chakravarty, *Inorg. Chim. Acta* **2010**, 363, 2743–2751.
- [8] T. Opstal, F. Verpoort, *Angew. Chem. Int. Ed.* **2003**, 42, 2876–2879; *Angew. Chem.* **2003**, 115, 2982.
- [9] G. Lyashenko, G. Saischek, M. E. Judmaier, M. Volpe, J. Baumgartner, F. Belaj, V. Jancik, R. Herbst-Irmer, N. C. Moesch-Zanetti, *Dalton Trans.* **2009**, 29, 5655–5665.
- [10] N. C. Moesch-Zanetti, D. Wurm, M. Volpe, G. Lyashenko, B. Harum, F. Belaj, J. Baumgartner, *Inorg. Chem.* **2010**, 49, 8914–8921.
- [11] a) R. Dinda, P. Sengupta, S. Ghosh, W. S. Sheldrick, *Eur. J. Inorg. Chem.* **2003**, 363–369; b) R. Dinda, P. Sengupta, S. Ghosh, H. Mayer-Figge, W. S. Sheldrick, *J. Chem. Soc., Dalton Trans.* **2002**, 4434–4439; c) W. Plass, *Eur. J. Inorg. Chem.* **1998**, 799–805; d) S. P. Dash, A. K. Panda, S. Pasayat, R. Dinda, A. Biswas, E. R. T. Tiekink, S. Mukhopadhyay, S. K. Bhutia, W. Kaminsky, E. Sinn, *RSC Adv.* **2015**, 5, 51852–51867.
- [12] M. Mancka, W. Plass, *Inorg. Chem. Commun.* **2007**, 10, 677–680.
- [13] R. Debel, A. Buchholz, W. Plass, *Z. Anorg. Allg. Chem.* **2008**, 634, 2291–2298.
- [14] K. Jeyakumar, D. K. Chand, *J. Chem. Sci.* **2009**, 121, 111–123.
- [15] M. R. Maurya, *Curr. Org. Chem.* **2012**, 16, 73–88.
- [16] R. D. Chakravathy, K. Suresh, V. Ramkumar, D. K. Chand, *Inorg. Chim. Acta* **2011**, 376, 57–63.
- [17] Z. Hu, X. Fu, Y. Li, *Inorg. Chem. Commun.* **2011**, 14, 497–501.
- [18] M. Herbert, F. Montilla, A. Galindo, *J. Mol. Catal. A* **2011**, 338, 111–120.
- [19] A. Rezaeifard, I. Sheikhshoae, N. Monadi, M. Alipour, *Polyhedron* **2010**, 29, 2703–2709.
- [20] I. Sheikhshoae, A. Rezaeifard, N. Monadi, S. Kaafi, *Polyhedron* **2009**, 28, 733–738.
- [21] A. Gunyar, D. Betz, M. Drees, E. Herdtweck, F. E. Kuhn, *J. Mol. Catal. A* **2010**, 331, 117–124.
- [22] W. Plass, *Z. Anorg. Allg. Chem.* **1997**, 623, 997–1005.
- [23] M. R. Maurya, S. Sikarwar, P. Manikandan, *Appl. Catal. A* **2006**, 315, 74–82.
- [24] A. J. Burke, *Coord. Chem. Rev.* **2008**, 252, 170–175.
- [25] K. R. Jain, W. A. Herrmann, F. E. Kuhn, *Coord. Chem. Rev.* **2008**, 252, 556–568.
- [26] K. C. Gupta, A. K. Sutar, *Coord. Chem. Rev.* **2008**, 252, 1420–1450.
- [27] B. Frédéric, *Coord. Chem. Rev.* **2003**, 236, 71–89.
- [28] a) M. Bagherzadeh, R. Latifi, L. Tahsini, V. Amani, A. Ellernand, L. K. Woo, *Polyhedron* **2009**, 28, 2517–2521; b) M. R. Maurya, A. Arya, P. Adao, J. C. Pessoa, *Appl. Catal. A* **2008**, 351, 239–252; c) M. Abrantes, I. S. Gonçalves, M. Pillinger, C. Vurchio, F. M. Cordero, A. Brandi, *Tetrahedron Lett.* **2011**, 52, 7079–7082; d) M. Bagherzadeh, M. Amini, A. Ellern, L. K. Woo, *Inorg. Chem. Commun.* **2012**, 15, 52–55; e) A. V. Biradar, M. K. Dongare, S. B. Umbarkar, *Tetrahedron Lett.* **2009**, 50, 2885–2888.
- [29] a) P. M. Reis, C. A. Gamelas, J. A. Brito, N. Saffon, M. Gomez, B. Royo, *Eur. J. Inorg. Chem.* **2011**, 666–673; b) C. Dinoi, M. Ciclosi, E. Manoury, L. Maron, L. Perrin, R. Poli, *Chem. Eur. J.* **2010**, 16, 9572–9584; c) K. A. Jorgensen, *Chem. Rev.* **1989**, 89, 431–458; d) M. E. Judmaier, C. Holzer, M. Volpe, N. C. Moesch-Zanetti, *Inorg. Chem.* **2012**, 51, 9956–9966; e) J. A. Schachner, P. Traar, C. Sala, M. Melcher, B. N. Harum, A. F. Sax, M. Volpe, F. Belaj, N. C. Moesch-Zanetti, *Inorg. Chem.* **2012**, 51, 7642–7649; f) M. E. Judmaier, C. H. Sala, F. Belaj, M. Volpe, N. C. Moesch-Zanetti, *New J. Chem.* **2013**, 37, 2139–2149; g) P. Traar, J. A. Schachner, B. Stanje, F. Belaj, N. C. Moesch-Zanetti, *J. Mol. Catal. A* **2014**, 385, 54–60; h) A. Günyar, D. Betz, M. Drees, E. Herdtweck, F. E. Kuhn, *J. Mol. Catal. A* **2010**, 331, 117–124; i) F. Barrière, *Coord. Chem. Rev.* **2003**, 236, 71–89; j) M. M. Farahani, F. Farzaneh, M. Ghandi, *Catal. Commun.* **2007**, 8, 6–10; k) J. Zhao, X. Zhou, A. M. Santos, E. Herdtweck, C. C. Romao, F. E. Kuhn, *Dalton Trans.* **2003**, 3736–3742; l) J. M. Sobczak, J. J. Ziolkowski, *Appl. Catal. A* **2003**, 248, 261–268; m) J. Pisk, D. Agustin, V. Vrdoljak, R. Poli, *Adv. Synth. Catal.* **2011**, 353, 2910–2914; n) X. Lei, N. Chelamalla, *Polyhedron* **2013**, 49, 244–251.
- [30] a) J. J. Boruah, S. P. Das, R. Borah, S. R. Gogoi, N. S. Islam, *Polyhedron* **2013**, 52, 246–254; b) S. Pasayat, S. P. Dash, S. Roy, R. Dinda, S. Dhaka, M. R. Maurya, W. Kaminsky, Y. P. Patil, M. Nethaji, *Polyhedron* **2014**, 67, 1–10; c) M. R. Maurya, S. Dhaka, F. Avecilla, *Polyhedron* **2014**, 67, 145–159.
- [31] a) M. Bagherzadeh, M. M. Haghdoost, M. Amini, P. G. Derakhshandeh, *Catal. Commun.* **2012**, 23, 14–19; b) M. Bagherzadeh, L. Tahsini, R. Latifi, A. Ellern, L. K. Woo, *Inorg. Chim. Acta* **2008**, 361, 2019–2024; c) G. Mohammadnezhad, R. Debel, W. Plass, *J. Mol. Catal. A* **2015**, 410, 160–167.
- [32] *Vanadium and its Role in Life, Metal Ions in Biological Systems* (Eds.: H. Sigel, A. Sigel), Marcel Dekker, New York, **1995**, vol. 31.
- [33] D. C. Crans, J. J. Smee, E. Gaidamauskas, L. Yang, *Chem. Rev.* **2004**, 104, 849–902.
- [34] A. S. Tracey, G. R. Willsky, E. S. Takeuchi, *Vanadium Chemistry, Biochemistry Pharmacology and Practical Applications*, CRC Press, Boca Raton, USA, **2007**.
- [35] D. Rehder, *Bioinorganic Vanadium Chemistry*, John Wiley & Sons, Ltd. Chichester, UK, UK, **2008**.
- [36] A. Butler, J. V. Walker, *Chem. Rev.* **1993**, 93, 1937–1944.
- [37] W. Plass, *Angew. Chem. Int. Ed.* **1999**, 38, 909–912; *Angew. Chem.* **1999**, 111, 960.
- [38] C. R. Cornman, E. P. Zovinka, M. H. Meixner, *Inorg. Chem.* **1995**, 34, 5099–5100.
- [39] K. H. Thompson, J. H. McNeill, C. Orvig, *Chem. Rev.* **1999**, 99, 2561–2572.
- [40] K. H. Thompson, B. D. Liboiron, Y. Sun, K. D. D. Bellman, V. Karunaratne, G. Rawji, J. Wheeler, K. Sutton, S. Bhanot, S. B. C. Cassidy, J. H. McNeill, V. G. Yuen, C. Orvig, *J. Biol. Inorg. Chem.* **2003**, 8, 66–74.
- [41] H. Yasui, Y. Adachi, A. Katoh, H. Sakurai, *J. Biol. Inorg. Chem.* **2007**, 12, 843–853.
- [42] Y. Shechter, I. Goldwasser, M. Mironchik, M. Fridkin, D. Gefel, *Coord. Chem. Rev.* **2003**, 237, 3–11.
- [43] A. M. B. Bastos, J. G. da Silva, P. I. S. Maia, V. M. Deflon, A. A. Batista, A. V. M. Ferreira, L. M. Botion, E. Niquet, H. Beraldo, *Polyhedron* **2008**, 27, 1787–1794.
- [44] R. R. Eady, *Coord. Chem. Rev.* **2003**, 237, 23–30.
- [45] a) K. Yamamoto, K. Oyaizu, E. Tsuchida, *J. Am. Chem. Soc.* **1996**, 118, 12665–12672; b) N. Mizuno, Y. Nakagawa, K. Yamaguchi, *J. Mol. Catal. A* **2006**, 251, 286–290; c) S. H. Hsieh, Y. P. Kuo, H. M. Gau, *Dalton Trans.* **2007**, 97; d) H. Somei, Y. Asano, T. Yoshida, S. Takizawa, H. Yamataka, H. Sasai, *Tetrahedron Lett.* **2004**, 45, 1841–1844; e) S. Takizawa, T. Katayama, H. Somei, Y. Asano, T. Yoshida, C. Kameyama, D. Rajesh, K. Onitsuka, T. Suzuki, M. Mikami, H. Yamatakay, D. Jayaprakash, H. Sasai, *Tetrahedron* **2008**, 64, 3361–3371; f) Q.-X. Guo, Z.-J. Wu, Z.-B. Luo, Q.-Z. Liu, J.-L. Ye, S.-W. Luo, L.-F. Cun, L.-Z. Gong, *J. Am. Chem. Soc.* **2007**, 129, 13927–13938; g) M. R. Maurya, S. Agarwal, C. Bader, D. Rehder, *Eur. J. Inorg. Chem.* **2005**, 147–157; h) M. R. Maurya, M. Kumar, A. Arya, *Catal. Commun.* **2008**, 10, 187–191; i) M. R. Maurya, A. A. Khan, A. Azam, A. Kumar, S. Ranjan, N. Mondal, J. C. Pessoa, *Eur. J. Inorg. Chem.* **2009**, 5377–5390; j) M. R. Maurya, P. Saini, A. Kumar, J. C. Pessoa, *Eur. J. Inorg. Chem.* **2011**, 4846–4861; k) M. R. Maurya, M. Bisht, F. Avecilla, *J. Mol. Catal. A* **2011**, 344, 18–27; l) M. R. Maurya, C. Haldar, A. A. Khan, A. Azam, A. Salahuddin, A. Kumar, J. C. Pessoa, *Eur. J. Inorg. Chem.* **2012**, 2560–2577; m) S. Patra, S. Chatterjee, T. K. Si, K. K. Mukherjee, *Dalton Trans.* **2013**, 42, 13425–13435; n) S. Parihar, R. N. Jadeja, V. K. Gupta, *RSC Adv.* **2014**, 4, 10295–10302; o) J. Becher, I. Seidel, W. Plass, D. Klemm, *Tetrahedron* **2006**, 62, 5675–5681; p) I. Lippold, K. Vlay, H. Görls, W. Plass, *J. Inorg. Biochem.* **2009**, 103, 480–486; q) M. Schulz, R. Debel, H. Görls, W. Plass, M. Westerhausen, *Inorg. Chim. Acta* **2011**, 365, 349–355.
- [46] S. Bhattacharya, T. Ghosh, *Transition Met. Chem.* **2002**, 27, 89–94.
- [47] S. Basu, G. Gupta, B. Das, K. M. Rao, *J. Organomet. Chem.* **2010**, 695, 2098–2104.

- [48] S. Priyarega, M. M. Tamizh, R. Karvembu, R. Prabhakaran, K. Natarajan, *J. Chem. Sci.* **2011**, *123*, 319–325.
- [49] M. H. Habibi, E. Shojaei, Y. Yamane, T. Suzuki, *J. Inorg. Organomet. Polym.* **2012**, *22*, 190–195.
- [50] A. A. Abdel Aziz, A. N. M. Salem, M. A. Sayed, M. M. Aboaly, *J. Mol. Struct.* **2012**, *1010*, 130–138.
- [51] J. Joseph, K. Nagashri, G. B. Janaki, *Eur. J. Med. Chem.* **2012**, *49*, 151–163.
- [52] A. Majumder, G. M. Rosair, A. Mallick, N. Chattopadhyay, S. Mitra, *Polyhedron* **2006**, *25*, 1753–1762.
- [53] A. R. Stefankiewicz, M. Wałęsa-Chorab, H. B. Szcześniak, V. Patroniak, M. Kubicki, Z. Hnatejko, J. Harrowfield, *Polyhedron* **2010**, *29*, 178–187.
- [54] D. Chatterjee, *J. Mol. Catal. A* **2009**, *310*, 174–179.
- [55] Y. Wong, D. K. P. Ng, H. K. Lee, *Inorg. Chem.* **2002**, *41*, 5276–5285.
- [56] a) T. Arumuganathan, R. Mayilmurugan, M. Volpe, N. C. Möscher-Zanetti, *Dalton Trans.* **2011**, *40*, 7850–7857; b) S. K. Kurapati, U. Ugandhar, S. Maloth, S. Pal, *Polyhedron* **2012**, *42*, 161–167.
- [57] O. A. M. Ali, S. M. El-Medani, D. A. Ahmed, D. A. Nassar, *J. Mol. Struct.* **2014**, *1074*, 713–722.
- [58] P. Prasad, P. K. Sasmal, I. Khan, P. Kondaiah, A. R. Chakravarty, *Inorg. Chim. Acta* **2011**, *372*, 79–87.
- [59] N. Pooransingh, E. Pomerantseva, M. Ebel, S. Jantzen, D. Rehder, T. Polenova, *Inorg. Chem.* **2003**, *42*, 1256–1266.
- [60] T. Birkel, A. Carbayo, J. V. Cuevas, G. García-Herbosa, A. Muñoz, *Eur. J. Inorg. Chem.* **2012**, 2259–2266.
- [61] B. T. Golding, J. M. Harrowfield, G. B. Robertson, A. M. Sargeson, P. O. Whimp, *J. Am. Chem. Soc.* **1974**, *96*, 3691–3692.
- [62] G. A. Stark, A. M. Arif, J. A. Gladysz, *Organometallics* **1994**, *13*, 4523–4530.
- [63] A. M. Arnaiz, A. Carbayo, J. V. Cuevas, V. Díez, G. García-Herbosa, R. González, A. Martínez, A. Muñoz, *Eur. J. Inorg. Chem.* **2007**, 4637–4644.
- [64] S. Gupta, S. Pal, A. K. Barik, S. Roy, A. Hazra, T. N. Mandal, R. J. Butcher, S. K. Kar, *Polyhedron* **2009**, *28*, 711–720.
- [65] S. K. Kurapati, S. Pal, *Dalton Trans.* **2015**, *44*, 2401–2408.
- [66] S. Pasayat, S. P. Dash, Saswati, P. K. Majhi, Y. P. Patil, M. Nethaji, H. R. Dash, S. Das, R. Dinda, *Polyhedron* **2012**, *38*, 198–204.
- [67] A. Sarkar, S. Pal, *Inorg. Chim. Acta* **2009**, *362*, 3807–3812.
- [68] K. P. Jensen, *Inorg. Chem.* **2008**, *47*, 10357–10365.
- [69] D. Marx, *ChemPhysChem* **2006**, *7*, 1848–1870.
- [70] M. L. Karahka, H. J. Kreuzer, *Biointerphases* **2013**, *8*, 13/1–13/9.
- [71] E. Grunwald, C. F. Jumper, S. Meiboom, *J. Am. Chem. Soc.* **1962**, *84*, 4664–4671.
- [72] P. A. Kollman, D. M. Hayes, *J. Am. Chem. Soc.* **1981**, *103*, 2955–2961.
- [73] J. A. Morrone, M. E. Tuckerman, *J. Chem. Phys.* **2002**, *117*, 4403–4413.
- [74] M. R. Maurya, U. Kumar, P. Manikandan, *Dalton Trans.* **2006**, 3561–3575.
- [75] M. R. Maurya, M. Kumar, U. Kumar, *J. Mol. Catal. A* **2007**, *273*, 133–143.
- [76] a) B. S. Lane, M. Vogt, V. J. De Rose, K. Burgess, *J. Am. Chem. Soc.* **2002**, *124*, 11946–11954; b) S. K. Maiti, S. Dinda, S. Banerjee, A. K. Mukherjee, R. Bharracharyya, *Eur. J. Inorg. Chem.* **2008**, 2038–2051; c) M. Bagherzadeh, M. Aminia, H. Parastar, M. Jalali-Heravi, A. Ellern, L. K. Woo, *Inorg. Chem. Commun.* **2012**, *20*, 86–89.
- [77] D. E. Richardson, H. Yao, K. M. Frank, D. A. Bennett, *J. Am. Chem. Soc.* **2000**, *122*, 1729–1739.
- [78] a) S. Nica, A. Pohlmann, W. Plass, *Eur. J. Inorg. Chem.* **2005**, 2032–2036; b) S. K. Maiti, S. Dinda, N. Gharah, R. Bhattacharyya, *New J. Chem.* **2006**, *30*, 479–489; c) S. Nica, M. Rudolph, I. Lippold, A. Buchholz, H. Görls, W. Plass, *J. Inorg. Biochem.* **2015**, 193–203.
- [79] G. J. J. Chen, J. W. Mc Donald, W. E. Newton, *Inorg. Chem.* **1976**, *15*, 2612–2615.
- [80] C. G. Pitt, Y. Bao, J. Thompson, M. C. Wani, H. Rosenkrantz, J. Metterville, *J. Med. Chem.* **1986**, *29*, 1231–1237.
- [81] S. Pasayat, *Ph. D. Thesis* (Chemistry of Oxomolybdenum Complexes with ON- and ONO-Donor Ligands), **2013**.
- [82] G. M. Sheldrick, *SHELXS-97, Program for Crystal Structure Determination*, University of Göttingen, Germany, **1997**.
- [83] G. M. Sheldrick, *SHELXL-97, Program for Refinement of Crystal Structures*, University of Göttingen, Germany, **1997**.
- [84] F. Neese, *WIRES Comput. Mol. Sci.* **2011**, *2*, 73–78.
- [85] a) J. Tao, J. P. Perdew, V. N. Staroverov, G. E. Scuseria, *Phys. Rev. Lett.* **2003**, *91*, 146401/1–146401/4; b) V. N. Staroverov, G. E. Scuseria, J. Tao, J. P. Perdew, *J. Chem. Phys.* **2003**, *119*, 12129–12137.
- [86] a) A. Schäfer, H. Horn, R. Ahlrichs, *J. Chem. Phys.* **1992**, *97*, 2571–2577; b) F. Weigend, R. Ahlrichs, *Phys. Chem. Chem. Phys.* **2005**, *7*, 3297–3305.
- [87] a) S. Grimme, J. Antony, S. Ehrlich, H. Krieg, *J. Chem. Phys.* **2010**, *132*, 154104/1–154104/19; b) S. Grimme, S. Ehrlich, L. Goerigk, *J. Comput. Chem.* **2011**, *32*, 1456–1465.
- [88] a) A. Klamt, G. Schüürmann, *J. Chem. Soc. Perkin Trans. 2* **1993**, *2*, 799–805; b) A. Klamt, *J. Phys. Chem.* **1996**, *100*, 3349–3353; c) A. Klamt, V. Jonas, *J. Chem. Phys.* **1996**, *105*, 9972–9981.
- [89] S. F. Boys, F. Bernardi, *Mol. Phys.* **1970**, *19*, 553–566.
- [90] TURBOMOLE, v. 6.6 (**2014**), a development of University of Karlsruhe, Germany and Forschungszentrum Karlsruhe GmbH, **1989–2007**, TURBOMOLE GmbH, since **2007**; available from <http://www.turbomole.com>.

Received: December 21, 2015
Published Online: July 3, 2016